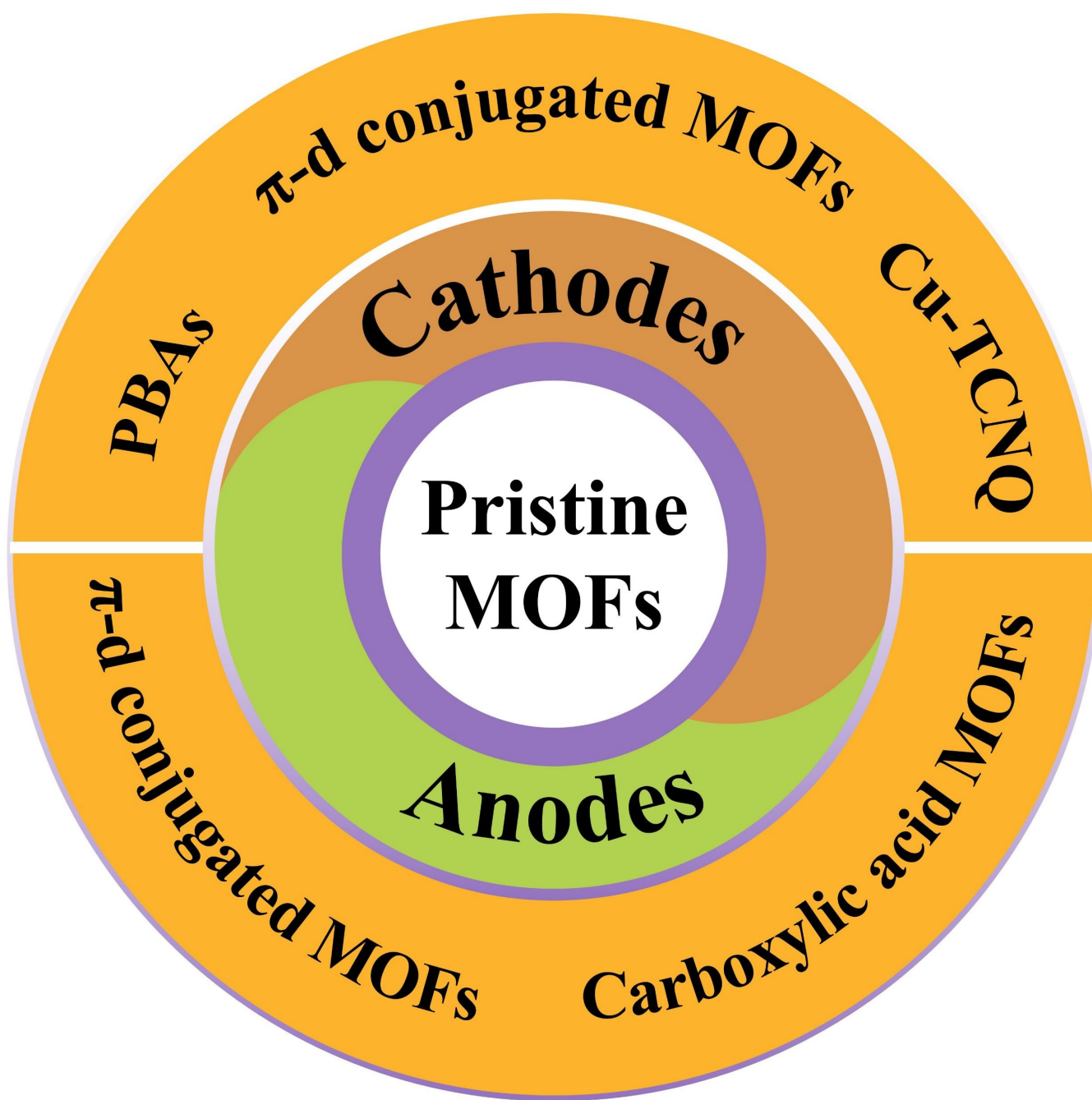


Pristine Metal-Organic Frameworks for Sodium-Ion Batteries: Past, Present, and Future

Chao Li,*^[a] Tao Ni,^[a] Min Yue,^[a] Shujun Li,^[a] and Qichun Zhang*^[b]



Owing to their adjustable redox-active sites, designable structures high porosity, and fully activated organic ligands, pristine metal-organic frameworks (MOFs) have been widely utilized as advanced electrode materials (i.e., both anodes and cathodes) for sodium-ion batteries (SIBs) to satisfied the insertion/extraction larger size and mass of Na^+ cations, achieving significant progresses with excellent electrochemical

performance in electrochemical energy storage devices. Here, the recent advances on pristine MOFs as anodes and cathodes for SIBs are summarized. A thorough investigation delves into the detailed characteristics, energy storage mechanisms, and electrochemical performance of diverse pristine MOFs for SIBs are also clarified. Furthermore, the outlooks on pristine MOF electrodes in SIBs are also provided.

1. Introduction

Metal-organic frameworks (MOFs),^[1–11] a well-established class of porous materials featuring metal cation/cluster nodes and organic ligand linkers, have demonstrated extensive applications.^[12–34] Coined by Yaghi,^[35] the term “MOFs” achieved prominence with the introduction of MOF-5, comprised of zinc oxide clusters connected by benzene dicarboxylate linkers, marked a groundbreaking achievement, showcasing the feasibility of designing crystalline materials with high surface areas and tunable pore sizes.^[36,37] This pivotal moment triggered an extensive exploration into new synthesis and applications, leading to diverse materials with varying properties. Especially, the structural diversity has enabled the creation of MOFs with varying surface areas, different pore sizes, and rich chemical functionalities, opening up many opportunities for applications in catalysis,^[38–43] gas separation and storage,^[44–47] and notably,^[48–66] particularly within the domain of energy storage,^[67–74] e.g., Li-ion batteries (LIBs), Na-ion batteries (SIBs), K-ion batteries (PIBs), multivalent metal-ion batteries^[75] (Such as Zinc-ion batteries, Aluminum-ion batteries, and so on), and supercapacitors.^[76]

Recently, SIBs have gained attention as a cost-effective alternative to LIBs, driven by the abundance of sodium (molar %, 2.1% for sodium and 0.005% for lithium), higher standard reduction potential (-2.71 V and -3.04 V vs. SHE (standard hydrogen electrode) for Na^+/Na and Li^+/Li , respectively), smaller solvated ionic radius, and better conductivity and mobility of Na-ion.^[77–81] However, challenges arise due to the larger size and mass of Na^+ cations, affecting the choice of electrode materials. Thus, MOFs, with their natural structural advantages of high porosity for Na-ion deintercalation, have emerged as promising electrode candidates for SIBs.^[82,83]

Over the years, the synthesis and optimization of MOF electrodes have become more sophisticated. However, MOFs always exhibit low electrical conductivity and low sodium-ions

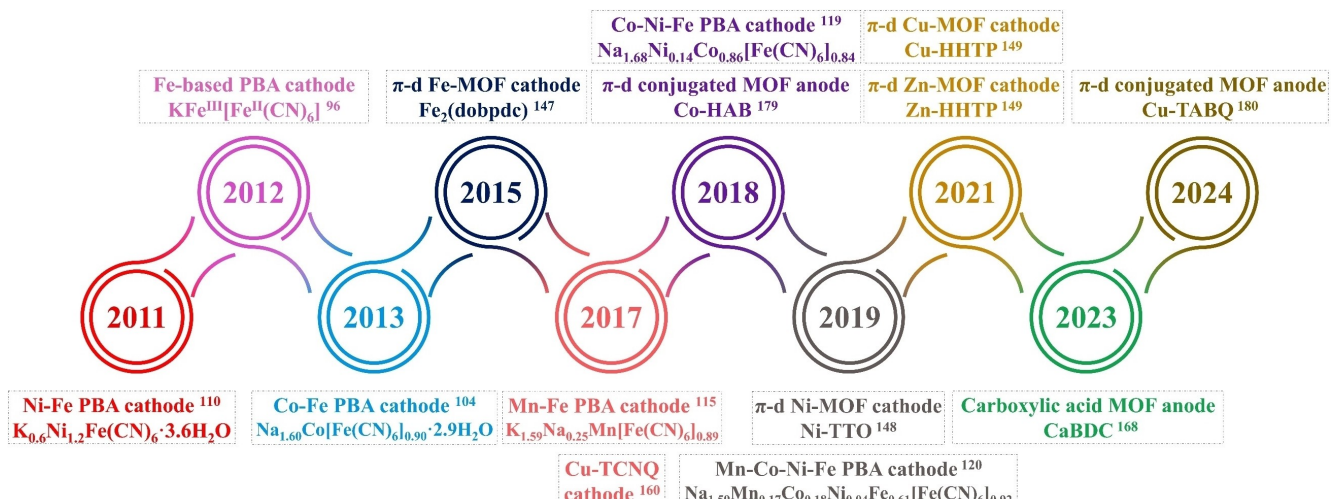
diffusion kinetics due to the inherently insulating or semi-conducting organic ligands and larger ionic radius of sodium-ions (1.12 Å) than that of lithium-ions (0.76 Å), which limited their detailed electrochemical properties in SIBs.^[84] Thus, researchers have developed numerous methods to control the chemical composition, chemical structure, particle size, shape, pore size, specific surface area size, and detailed electrochemical performances of MOFs,^[85] as well as enhancing the natural conductivity, electrochemical stability, and energy density of MOF electrodes, such as the design of high-quality nanocrystal Prussian blue analogs and high conductively π -d conjugated MOF.^[86,87] In fact, in previous reviews on MOF-related electrodes for SIBs,^[79,84–85] substantial attention has been devoted to the electrochemical performances and Na-ion storage mechanisms of MOF derivatives, including metal oxides, sulfides, phosphides, and selenides. This focus often overlooks the investigation of pristine MOF electrodes.^[82,87,88] In such cases, the conversion of MOFs into their derivatives through calcination or other battery-related treatments results in the sacrifice of organic ligands. This transformation significantly reduces the number of active sites in the original pristine MOF structures, leading to several challenges such as precursor waste, increased industrial costs, and impracticality for widespread application. In contrast, the intrinsic organic ligands within pristine MOFs can be fully activated to provide the contribution to energy storage devices. A thorough comprehension of the storage mechanisms for both organic ligands and metal cations in pristine MOFs offers valuable insights into advancing high-performance MOF-based electrodes in electrochemical energy batteries. Thus, this review comprehensively surveys recent advances in pristine MOF anodes and cathodes for application in SIBs (see detail in Scheme 1). Additionally, detailed explorations of characteristics, energy storage mechanisms, detailed electrochemical performance, and future outlooks of MOF electrodes for SIBs are also clarified.

2. Pristine MOFs as Cathodes for SIBs

Several pristine MOFs, such as Prussian blue analogs (PBAs), π -d conjugated MOFs, and Copper 7,7,8,8-tetracyanoquinodimethane (Cu-TCNQ), have recently emerged as promising cathode candidates in SIBs. These pristine MOFs have been demonstrated to show outstanding electrochemical performance and exhibit notable energy storage capabilities. Their attractiveness stems from a harmonious blend of high capacities and relatively low cost, positioning them favorably for applications in electric vehicles, grid energy storage, and portable electronic devices.

[a] Dr. C. Li, T. Ni, Dr. M. Yue, Dr. S. Li
School of Physics and Electronic Engineering
Sichuan University of Science & Engineering
Yibin 644000, PR China
E-mail: chaolicc@outlook.com

[b] Prof. Q. Zhang
Department of Materials Science and Engineering, Department of Chemistry,
Center of Super-Diamond and Advanced Films (COSDAF) & Hong Kong Institute of Clean Energy
City University of Hong Kong
Hong Kong SAR 999077, PR China
E-mail: qiczhang@cityu.edu.hk



Scheme 1. Milestone timeline of pristine MOF electrodes for Na-ion batteries.

The distinctive properties of MOF cathodes, particularly their facilitation of multi-electron transfer processes and redox-active sites, thereby significantly improving the overall electrochemical performance of energy storage devices.

2.1. PBA Cathodes

As representative cathodes for SIBs, PBAs have undergone extensive investigation.^[89] PBAs trace their origins in the chemical compound Prussian blue, a deep blue pigment with the chemical formula $Fe[Fe(CN)_6]_3$.^[90] Structurally resembling Prussian blue, PBAs comprise metal cations coordinated with cyanide ligands, forming an open framework characterized by tunable porosity, high surface area, and redox activity. These intriguing properties make PBAs highly promising as cathode materials for SIBs.^[91]

2.1.1. Characteristics and Energy Storage Mechanisms

PBAs have gained recognition as potential cathodes for SIBs because of their unique structure and electrochemical proper-

ties. Constructed with a cubic crystal structure, PBAs involve metal cations (e.g., Fe^{2+} and Fe^{3+}) coordinated with hexacyanometalate anions (e.g., $[Fe(CN)_6]^{4-}$ and $[Fe(CN)_6]^{3-}$), allowing reversible Na-ions extraction/insertion with an open framework structure. The generalized chemical structure of PBAs could be symbolized as $A_xM_H^{III}[M_L^{II}(CN)_6]_{1-y} \cdot \square_y \cdot nH_2O$,^[92] where A typically demotes alkali metal of Li, Na, or K, M_H/M_L signifying the transition metal, encompassing Fe, Co, Ni, Mn, Cu, or Zn, and \square representing vacancies in PBAs.^[93] As shown in Figure 1, PBAs exhibit two discernible oxidation states of transition metal: high spin M_H (HS- M_H) and low spin M_L (LS- M_L), usually exhibiting a space group symmetry of Fm-3m. Notably, HS- M_H is located adjacent to nitrogen (N) atoms in M_HN_6 octahedra, while LS- M_L is coordinated with carbon (C) atoms in M_LC_6 octahedra. Moreover, numerous vacancies within the framework are occupied by H_2O molecules to maintain overall structural neutrality, while other vacancies persist to accommodate the diverse quantities and mixed valence between M_H and M_L ,^[94] in which, the presence of vacancies could affect the content of M_L^{II} as well as the detail amount of A-ions, the randomly distributed vacancies could result in structural distortions and defects causing structural collapse, and the crystalline H_2O molecules could cause side reactions with the electrolyte. Thus, research-



Chao Li is currently a lecturer at the School of Physics and Electronic Engineering, Sichuan University of Science & Engineering. He received his Ph.D. degree at the School of Materials and Energy, University of Electronic Science and Technology of China. From 2019 to 2020, he joined Prof. Qichun Zhang's group as a joint PhD student at the School of Materials Science and Engineering, Nanyang Technological University, Singapore. His research interests involve organic energy storage materials and their applications, particularly, novel electrode materials as well as new designs for energy storage devices.



Qichun Zhang is a full professor in Department of Materials Science and Engineering at City University of Hong Kong, China. Before moved to Hong Kong, he was a tenured associate professor at the School of Materials Science and Engineering, Nanyang Technological University (Singapore). His research interests include carbon-rich conjugated materials and their applications for optoelectronic and semiconductor devices (H index: 120).

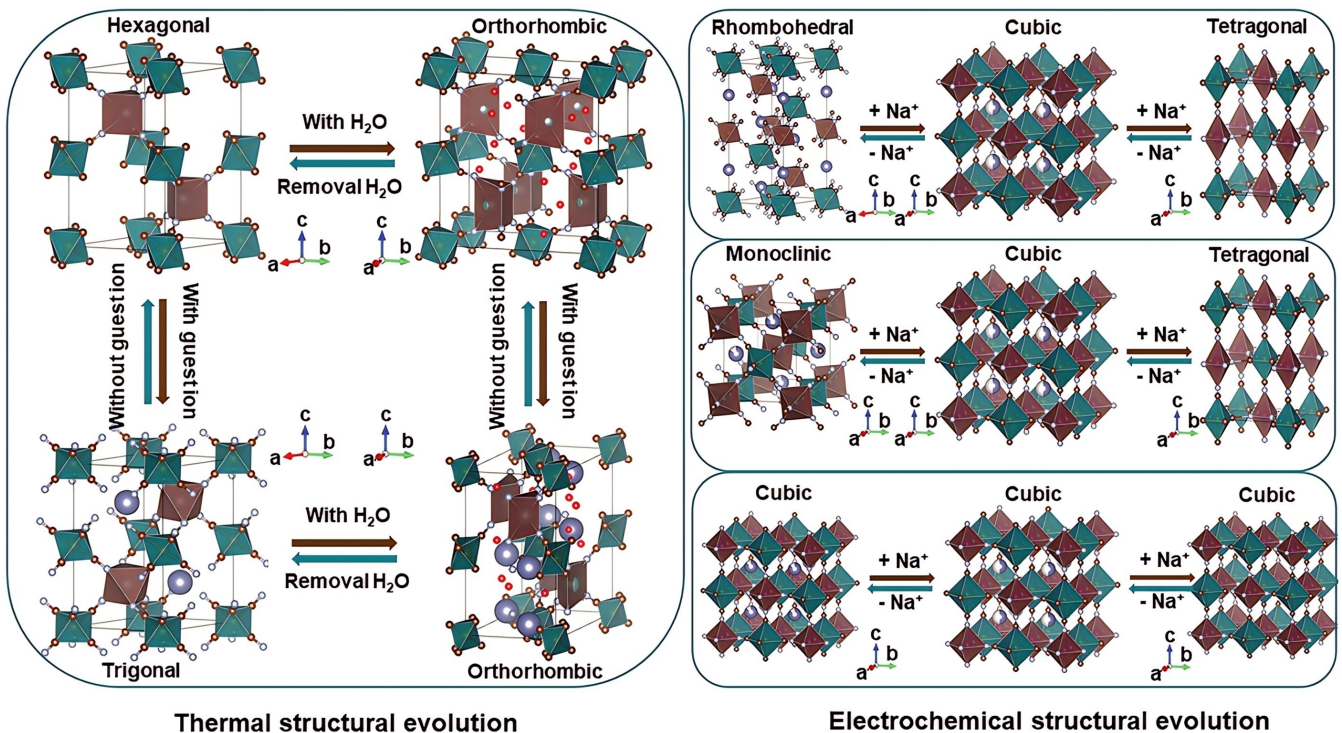
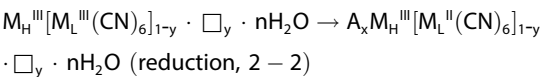
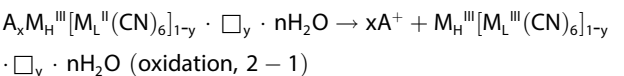


Figure 1. The chemical structure and atomic position of PBAs, $A_xM_H^{III}[M_L^{II}(CN)_6]_{1-y} \cdot \square_y \cdot nH_2O$, and the structural evolution with the intercalation and extraction of Na^+ . Reproduced with permission from Ref. [94]. Copyright (2022) Wiley-VCH.

ers have devoted many efforts to minimizing crystal defects and removing crystalline H_2O during the synthesis of PBAs. As well as we know, one common method for synthesizing PBAs involves co-precipitating metal salts in the presence of a reducing agent. This method typically entails mixing aqueous solutions of metal salts (particularly iron and hexacyanometallate precursors), resulting in PBAs formation. Additionally, the sol-gel method enables controlled PBA synthesis through the hydrolysis and polycondensation of metal precursors in a solution, offering superior control over particle size and morphology. Moreover, PBAs can be synthesized via ion-exchange reactions, where alkali metal ions (such as Li^+ , Na^+ , and K^+) replace metal ions in the Prussian blue lattice, facilitating tailored composition for specific applications. Meanwhile, introducing defects or substitutions in the Prussian blue lattice can enhance the electrochemical performance of PBAs by providing additional sites for sodium-ion storage and tailoring the nanostructure, such as nanocubes, nanowires, or nanoparticles, thereby enhancing the specific surface area and promoting faster ion diffusion. The energy storage mechanisms of PBAs for SIBs rely on the transformation and sodium-ion insertion/extraction between Prussian blue and Prussian white. Notably, the reversible transformation between Prussian white (ferrous state) and Prussian blue (ferric state) during cycling serves as a key mechanism for sodium-ion storage (Figure 1). Additionally, the discharge/charge process entails the reversible extraction/insertion of Na -ions, which intercalate into the Prussian blue lattice, triggering redox reactions with metal centers (e.g., Fe^{2+}/Fe^{3+}). In detail, the varieties of transition

metals in M_H play a crucial role in determining the detailed Na -ions storage mechanisms and electrochemical performance of PBAs in SIBs. When M_H denotes the electrochemically inert transition metal like Ni, Cu, or Zn, in such PBAs, the exclusive redox-active couple is solitary M_L^{III}/M_L^{II} , resulting in notable cyclic disabilities and poor rate performance but with limited theoretical specific capacities. Conversely, if M_H represents redox-active transition metals like Mn, Fe, or Co, these PBAs exhibit improved theoretical specific capacity based on the dual electron redox reactions, involving both M_H^{III}/M_H^{II} and M_L^{III}/M_L^{II} redox active couples compared to counterparts with a solitary redox-active couple. Therefore, both chemical composition and chemical structure could significantly influence the electrochemical properties of PBAs. The electrochemical mechanism of PBA cathodes could be elucidated as follows:



2.1.2. PBA Cathodes for SIBs

PBAs have emerged as highly promising cathode materials for SIBs, offering distinct advantages in terms of stability, high capacity, and cost-effectiveness. The representative types of PBAs, namely Fe-based PBAs and heterometallic PBAs, function effectively as cathodes for SIBs, demonstrating satisfactory electrochemical properties. As the Fe-based PBA cathode, $KFe^{III}[Fe^{II}(CN)_6]$, synthesized by Goodenough et al through combining Fe^{2+} salt and $K_3Fe(CN)_6$, exhibited a notable reversible capacity (100 mAh g^{-1}), indicating that the $Fe^{(II)}-N\equiv C-Fe^{(III)}$ bond length provided by the linear $(C\equiv N)^-$ molecule could facilitate Na^+ cations reversible insertion/extraction in the vacant large-ion sites, as displayed in Figure 2a. Subsequently, to enhance electrochemical performance, researchers have implemented strategies such as harnessing high-crystal Fe-based PBA nanostructures. For example, Yang et al. employed single-crystal Fe-based PBA nanoparticles, $Fe^{III}Fe^{III}(CN)_6$,^[96] as cathode materials for SIBs, achieving exceptional rate capabilities and superior cyclability capacity retentions. Guo et al. utilized high-quality nanocrystals of Fe-based PBA, i.e., $Na_{0.61}Fe[Fe(CN)_6]_{0.94}$,^[97] demonstrating exceptional long-cycle stability as cathodes for SIBs. Concurrently, Na-rich Fe-based PBAs, noted as Na-rich $Na_xFe[Fe(CN)_6]$ ($x \sim 2$) and characterized by minimal $Fe(CN)_6$ vacancies, have also shown improved electrochemical properties attributed to their rich Na-ion content, well-defined crystallinity, and nano-scaled particle size, as reported by Goodenough et al.,^[98] Huang et al.,^[99] and Dou et al.^[100] To further augment the long-cycle stability and improve the specific capacity of Fe-based PBA compounds,

conductive compounding modifications have been explored. For example, Jiang et al.^[101] coated Fe-based PBA with reduced graphene oxide (RGO), while Yang et al. composited carbon powder and Fe-based PBAs via mechanical ball-milling.^[102]

Within the realm of Fe-based PBAs, heterometallic PBAs including Co–Fe PBAs, Ni–Fe PBAs, Mn–Fe PBAs, Co–Ni–Fe PBAs, and Mn–Co–Ni–Fe PBAs, have attracted substantial attention as prominent cathodes for SIBs.^[103] As for Co–Fe PBA cathodes, a notable example, namely $Na_{1.60}Co[Fe(CN)_6]_{0.90}\cdot 2.9H_2O$, synthesized by Moritomo et al.,^[104] belongs to a $Fm-3m$ space group, manifesting a reversible capacity of 138 mAh g^{-1} within 75 mA g^{-1} rooted in a two-electron reaction of Co^{3+}/Co^{2+} and Fe^{3+}/Fe^{2+} redox couples, as demonstrated in Figure 2b. Furthermore, a range of Co–Fe PBAs, such as $K_{1.84}Co[Fe(CN)_6]_{0.89}\cdot \square_{0.11}$,^[105] $Na_{1.85}Co[Fe(CN)_6]_{0.99}\cdot 2.5H_2O$,^[106] $Na_{1.87}Co[Fe(CN)_6]_{0.98}\cdot 2.2H_2O$,^[107] and highly crystallized $Na_{1.85}Co[Fe(CN)_6]_{0.99}\cdot \square_{0.01}\cdot 1.9H_2O$,^[108] have been showcased as cathode materials for SIBs based on the redox reactions involving Co^{3+}/Co^{2+} and Fe^{3+}/Fe^{2+} couples.^[108] Similarly, extensive design and exploration efforts have been directed towards Ni–Fe PBAs as cathode materials for SIBs, capitalizing on the exclusive redox-activity Fe^{2+}/Fe^{3+} redox couple, while the non-participating redox reaction of Ni^{2+}/Ni^{3+} in the 2.0–4.2 V voltage windows, resulting in limited capacities below 100 mAh g^{-1} .^[95] For example, as shown in Figure 2c, Komaba et al.^[109] exposed Na-rich Ni–Fe PBAs, i.e., $Na_{1.20}Ni[Fe(CN)_6]_{0.65}$, obtaining a modest capacity of 66 mAh g^{-1} at 30 mA g^{-1} . Among them, various other Ni–Fe PBAs, such as $K_{0.6}Ni_{1.2}Fe(CN)_6\cdot 3.6H_2O$,^[110] $K_{0.09}Ni[Fe(CN)_6]_{0.71}\cdot 6H_2O$,^[111] $Na_{1.94}Ni_{1.03}Fe(CN)_6\cdot 4.8H_2O$,^[112] etched $Na_{1.11}Ni_{1.03}Fe(CN)_6\cdot 0.71H_2O$,^[113] $KNiFe(CN)_6$,^[95] and $Na_{1.82}Ni[Fe(CN)_6]_{0.85}\cdot 2.5H_2O$,^[114] have also been reported.

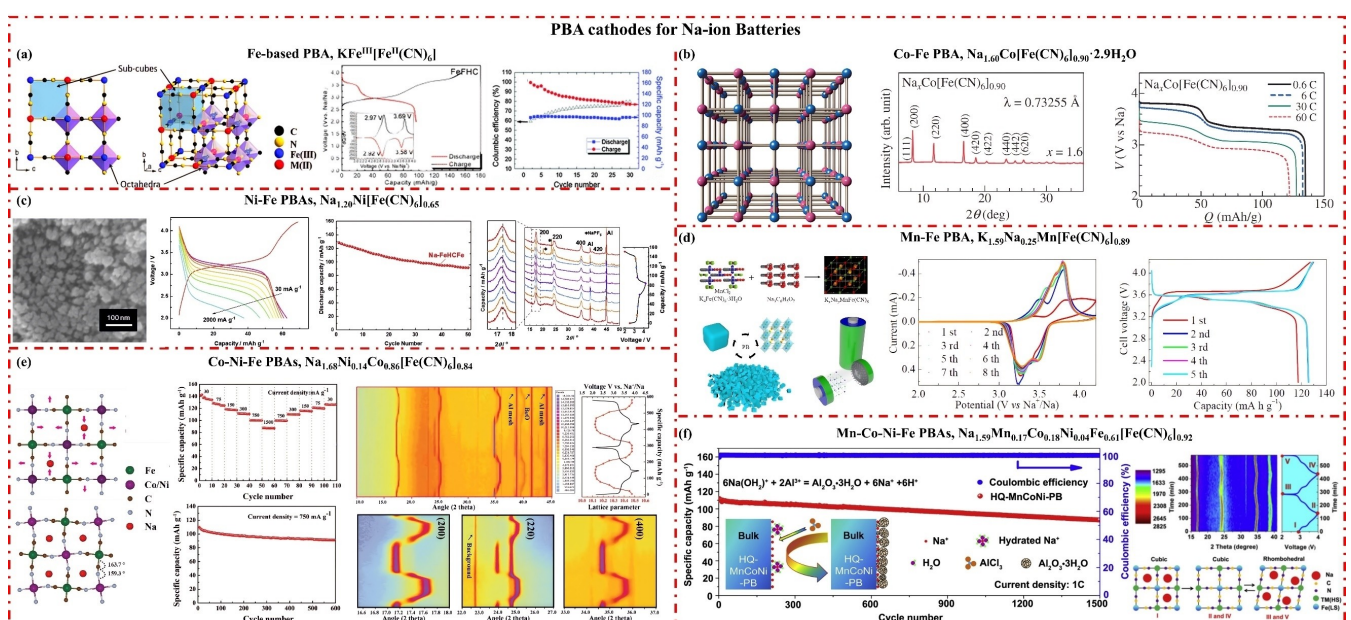


Figure 2. The structure characteristics and electrochemical performance of PBA cathodes for Na-ion batteries. a) Fe-based PBA, $KFe^{III}[Fe^{II}(CN)_6]$. Reproduced with permission from Ref. [95]. Copyright (2012) Royal Society of Chemistry; b) Co–Fe PBA, $Na_{1.60}Co[Fe(CN)_6]_{0.90}\cdot 2.9H_2O$. Reproduced with permission from Ref. [104]. Copyright (2013) Japan Society of Applied Physics; c) Ni–Fe PBAs, $Na_{1.20}Ni[Fe(CN)_6]_{0.65}$. Reproduced with permission from Ref. [109]. Copyright (2018) Elsevier; d) Mn–Fe PBA, $K_{1.59}Na_{0.25}Mn[Fe(CN)_6]_{0.89}$. Reproduced with permission from Ref. [115]. Copyright (2017) Royal Society of Chemistry; e) Co–Ni–Fe PBAs, $Na_{1.68}Ni_{0.14}Co_{0.86}[Fe(CN)_6]_{0.84}$. Reproduced with permission from Ref. [119]. Copyright (2018) Wiley-VCH; f) Mn–Co–Ni–Fe PBAs, $Na_{1.59}Mn_{0.17}Co_{0.18}Ni_{0.04}Fe_{0.61}[Fe(CN)_6]_{0.92}$. Reproduced with permission from Ref. [120]. Copyright (2019) Elsevier.

$(\text{CN})_6]_{0.90} \cdot \square_{0.10} \cdot 2.7\text{H}_2\text{O}$ ^[114] have been subsequently developed as cathodes for SIBs, however, the capacities of all Ni–Fe PBA cathodes remained below 100 mAh g⁻¹.

Furthermore, Mn–Fe PBA cathodes, akin to Co–Fe PBAs and Ni–Fe PBAs counterparts, have been explored as electrodes for SIBs. For example, as depicted in Figure 2d, Liu et al.^[115] employed a co-precipitation method to design a Mn–Fe PBA cathode, namely $\text{K}_{1.59}\text{Na}_{0.25}\text{Mn}[\text{Fe}(\text{CN})_6]_{0.89}$, resulting in a noteworthy capacity of 133.3 mAh g⁻¹ within 20 mA g⁻¹. Meanwhile, various Mn–Fe PBA cathodes, such as $\text{Na}_{1.80}\text{Mn}[\text{Fe}(\text{CN})_6]_{0.98}$,^[116] $\text{Na}_{1.92}\text{Mn}[\text{Fe}(\text{CN})_6]_{0.98}$,^[117] and $\text{Na}_{1.66}\text{Mn}[\text{Fe}(\text{CN})_6]_{0.94}$,^[118] have both demonstrated satisfactory electrochemical performances attributed to the redox reactions involving $\text{Fe}^{3+}/\text{Fe}^{2+}$ and $\text{Mn}^{3+}/\text{Mn}^{2+}$ couples while employed in SIBs. Additionally, the Co–Ni–Fe PBA cathodes and Mn–Co–Ni–Fe PBA cathodes have both been investigated for SIBs, such as $\text{Na}_{1.65}\text{Ni}_{0.14}\text{Co}_{0.86}[\text{Fe}(\text{CN})_6]_{0.84}$,^[119] and $\text{Na}_{1.59}\text{Mn}_{0.17}\text{Co}_{0.18}\text{Ni}_{0.04}\text{Fe}_{0.61}[\text{Fe}(\text{CN})_6]_{0.92}$,^[120] attributed to the redox reactions involving $\text{Co}^{3+}/\text{Co}^{2+}$ and $\text{Fe}^{3+}/\text{Fe}^{2+}$, $\text{Fe}^{3+}/\text{Fe}^{2+}$ and $\text{Mn}^{3+}/\text{Mn}^{2+}$ couples, obtained an impressive capacities of 145 mAh g⁻¹ within 30 mA g⁻¹ and 113 mAh g⁻¹ within 17 mA g⁻¹, as illustrated in Figures 2e and 2f, respectively.

In brief, PBAs have emerged as prominent candidates for cathode materials in various SIBs. Their outstanding electrochemical performance primarily results from the redox reactions involving $\text{Fe}^{3+}/\text{Fe}^{2+}$ couples, accompanied by the redox reactions of $\text{Co}^{3+}/\text{Co}^{2+}$ and $\text{Mn}^{3+}/\text{Mn}^{2+}$ couples, which was determined by the detailed chemical composition and chemical structure of PBAs, especially the types of M_H. Within PBAs, several factors such as crystal structure, micromorphology, H₂O content in crystal, A⁺ content as well as conductivity, are pivotal in shaping the detailed electrochemical performances of SIBs. As a result, achieving exceptional electrochemical performance hinges on the carefully designing high-quality nanocrystal PBAs involving minimizing crystal H₂O content, restricting Fe(CN)₆ vacancies, and ensuring an abundance of redox-active transition metal ions. Such meticulous design considerations are crucial for optimizing the performance of SIBs utilizing PBAs as cathode materials.

2.2. π-d Conjugated MOF Cathodes

In recent years, there has been increased attention on π-d conjugated MOFs, driven by their distinctive molecular architecture.^[121] π-d conjugated MOFs always comprise organic ligands and transition metal ions featuring oxygen, sulfur, and nitrogen ligation sites, allowing for electrons in a conjugated fashion. Meanwhile, the incorporation of π-conjugated fashion could result in natural high-conductive than traditional MOFs, such as MILs or ZIFs. The research area that involves the utilization of ligands, which could donate electron density to the metal ions center via π bonds has progressively gained prominence, offering several advantages such as design versatility, flexibility, low cost, and applicability across various domains, including sensing,^[122] drug delivery,^[123] catalysis,^[124,125] gas separation,^[126] magnetic properties,^[127] and electrochemical applications.^[128–132]

2.2.1. Characteristics and Energy Storage Mechanisms

The synthesis of π-d conjugated MOFs involves solvothermal methods, incorporating transition metal cations and organic ligands featuring oxygen, sulfur, or nitrogen ligation sites. Meanwhile, reaction conditions (i.e., pH value, reaction time, and temperature) control the resulting structure, characteristics, and performance of π-d MOFs. Additionally, the π-conjugated organic ligands impart unique electronic properties to the MOFs, including conductivity and optical characteristics. Different categories of π-d conjugated MOFs,^[133–137] e.g., π-d Fe-MOFs, π-d Co-MOFs, π-d Ni-MOFs, π-d Zn-MOFs, and π-d Cu-MOFs, have found widespread applications,^[138–143] especially as cathodes for SIBs thanks to their advantageous structural features.^[144] When delivered as cathodes for SIBs, the energy storage mechanisms of conductive π-d conjugated MOFs contribute to the redox reaction of C=O/C–O, C=S/C–S, C=N/C–N redox couples or along with the redox reaction of transition metal ions. Meanwhile, the detailed chemical composition of π-d conjugated MOFs could impact the detailed energy storage mechanisms and finally affect the detailed electrochemical properties. When the π-d conjugated MOFs contain the electrochemically inert metal ions, the energy storage mechanisms of such π-d conjugated MOFs could only rely on the redox-active C=O/C–O, C=S/C–S, or C=N/C–N couples, leading to limited theoretical specific capacities but notable cyclic disabilities and rate performance. While, if π-d conjugated MOFs contain redox-active metal ions, such as Cu²⁺, these energy storage mechanisms could both relying on the redox-active C=O/C–O, C=S/C–S, or C=N/C–N couples, and redox-active metal ions (such as Cu^{2+}/Cu⁺), resulting in enhanced specific capacity.}

2.2.2. π-d Conjugated MOF Cathodes for SIBs

π-d Conjugated MOFs have recently emerged as cathode materials for SIBs, leveraging redox reactions involving organic ligand sites or along with transition metal ions ($\text{M}^{3+}/\text{M}^{2+}$ or M^{2+}/M^+) couples, including π-d conjugated Fe-MOF cathodes, π-d conjugated Ni-MOF cathodes, π-d conjugated Cu-MOF cathodes, and so on.

For instance, Song and coworkers introduced a novel π-d Fe-MOF, $\text{Fe}_2(\text{DHBQ})_3$,^[145] eliminating the embedded (NBu₄)⁺ cation from (NBu₄)₂Fe₂(DHBQ)₃.^[146] As shown in Figure 3a, $\text{Fe}_2(\text{DHBQ})_3$, consisting of Fe³⁺ and DHBQ²⁻ within *P*-1 space group, exhibited a substantial theoretical capacity (408 mAh g⁻¹) with the redox reaction of $\text{Fe}^{3+}/\text{Fe}^{2+}$ and DHBQ²⁻/DHBQ⁴⁻ couples and an impressive electronic conductivity (1.1×10^{-4} S cm⁻¹), resulting in a significant reversible capacity (264 mAh g⁻¹ at 50 mA g⁻¹) along with a substantial energy density (560 Wh kg⁻¹). Furthermore, other π-d Fe-MOF cathode, i.e., $\text{Fe}_2(\text{dobpdc})$,^[147] constructed with 4,4'-dioxidobiphenyl-3,3'-dicarboxylate (dobpdc), was utilized as electrodes for sodium dual-ion batteries and Li-ion batteries, exhibiting topotactic oxidative insertion reactions with weakly BF₄⁻ and PF₆⁻ coordinating anions.

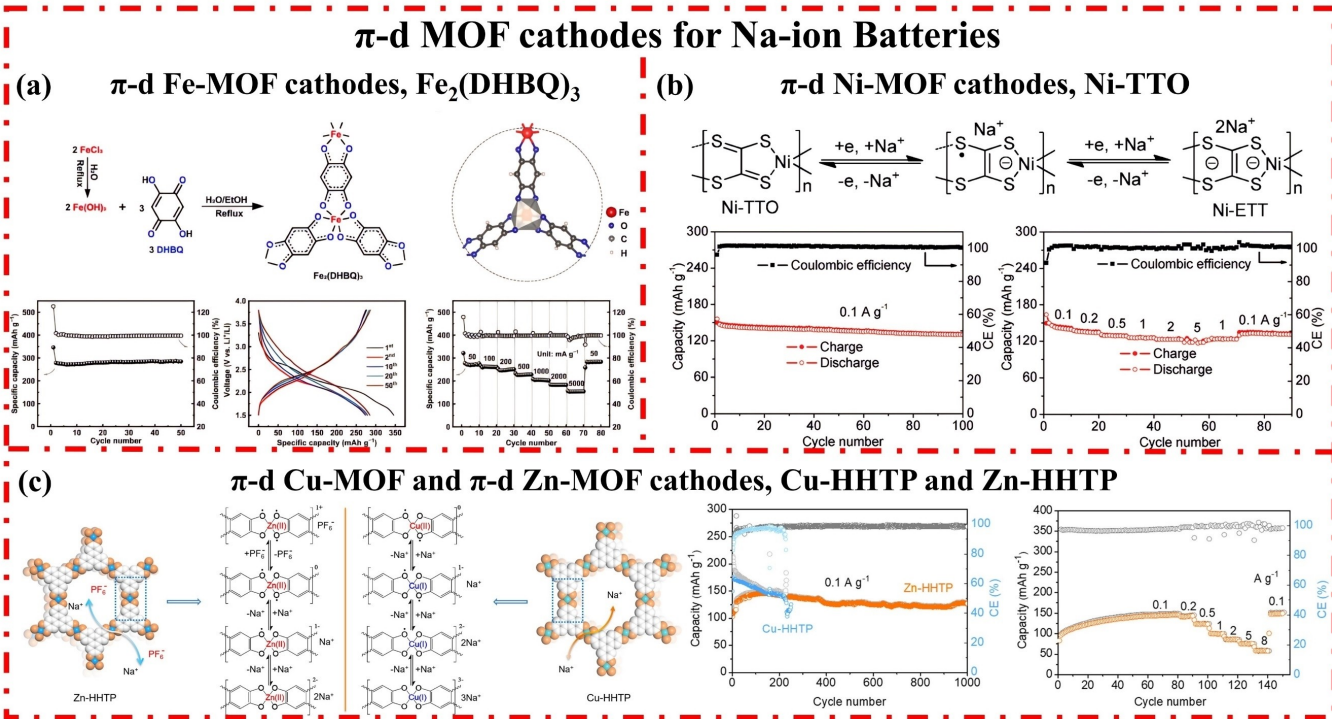


Figure 3. The structure characteristics and electrochemical performance of π -d conjugated MOF cathodes for Na-ion batteries. a) π -d Fe-MOF cathodes, $\text{Fe}_2(\text{DHBQ})_3$. Reproduced with permission from Ref. [146]. Copyright (2022) Elsevier. b) π -d Ni-MOF cathodes, Ni-TTO. Reproduced with permission from Ref. [148]. Copyright (2019) Royal Society of Chemistry. c) π -d Cu-MOF and π -d Zn-MOF cathodes, Cu-HHTP and Zn-HHTP, respectively. Reproduced with permission from Ref. [149]. Copyright (2021) Wiley-VCH.

Furthermore, π -d Ni-MOF cathodes have also been used in novel SIBs, such as Ni-TTO,^[148] based on ethenetetrathiolate (ETT) ligand with sulfur as ligating atoms. As demonstrated in Figure 3b, during the discharging/charging process along with Na^+ ions insertion/extraction, Ni-TTO could be reversibly converted to Ni-ETT. Meanwhile, owing to the impressive diffusion coefficient of Na-ion (approximately $10^{-1} \text{ cm}^2 \text{s}^{-1}$) and substantial conductivity (approximately 30 Scm^{-1}), Ni-TTO gained high capacities of 155 mAh g^{-1} at 100 mA g^{-1} and 118 mAh g^{-1} at $5,000 \text{ mA g}^{-1}$, respectively.

Moreover, as well as π -d Fe-MOFs and π -d Ni-MOFs, π -d Cu-MOF and π -d Zn-MOF could also be employed as cathodes for SIBs. For instance, Wang and coworkers designed both π -d Cu-MOF and π -d Zn-MOF^[149] based on the same organic ligands of 2,3,6,7,10,11-hexahydroxytriphenylene (HHTP), finding that the π -d Cu-MOF, namely Cu-HHTP, obtained poor long-term cycle life compared with the π -d Zn-MOF (Zn-HHTP) with the same organic ligands of HHTP due to both redox reaction of Cu^+ metal ions and HHTP ligands in Cu-HHTP, while only the redox reaction of $\text{HHTP}^{2-}/\text{HHTP}^{4-}$ in Zn-HHTP (Figure 3c), highlighting the significance of understanding the redox mechanisms would provide valuable insights for further designing high-performance π -d MOFs based SIBs.

Within the domain of π -d MOF cathodes, prominent variants encompass π -d Fe-MOFs, π -d Ni-MOFs, π -d Cu-MOF, and π -d Zn-MOF cathodes, collectively garnering substantial attention in the realm of SIBs. However, challenges related to crystal structural analysis, chemical composition design, synthesis

scalability, and a comprehensive understanding of electrochemical mechanisms need to be addressed.

2.3. Other Cathodes

The MIL MOFs, notably MIL Fe-MOFs, stand out as prominent representatives in the realm of MOFs. Their appeal lies in a myriad of advantages, including flexible pore structure, abundant adsorption sites, and exceptionally large specific surface area. These features have garnered increasing attention, positioning MIL MOFs, particularly the MIL Fe-MOFs leveraging the redox reaction of $\text{Fe}^{2+}/\text{Fe}^{3+}$ couple, as optimal cathode adsorbents for Li-ion Batteries (LIBs).^[86,150-152] However, despite these advantages, various MIL MOF cathodes, such as MIL-53(Fe)· H_2O ,^[153] MIL-53(Fe)_quinone,^[154] MIL-68(Fe),^[155] MIL-101(Fe),^[156,157] and MIL-116(Fe),^[158] have demonstrated relatively poor electrochemical performance in LIBs, limiting their broader application as cathodes within other alkali metal-ion batteries like SIBs. Recently, only one type of MIL MOF cathodes, namely MIL-100(Fe),^[159] has been employed in SIBs, without a doubt, MIL-100(Fe) cathodes gained poor performance with only 20 mAh g^{-1} at 0.1 C under the voltage ranging from 1.5 V to 4.0 V .

In the realm of novel MOF cathodes, CuTCNQ has emerged as a promising electrode for SIBs. Different from the MIL Fe-MOFs, CuTCNQ shows larger pores, higher redox potentials, and enhanced specific capacities, contributing to the both redox-

active Cu^{2+} and TCNQ^{2-} in CuTCNQ , while solitary $\text{Fe}^{2+}/\text{Fe}^{3+}$ couple in MIL Fe-MOFs. For example, as demonstrated in Figure 4a, Huang et al.^[160] introduced $\text{Cu}-\text{TCNQ}$ as an innovative cathode material for SIBs, featuring the $P2/n$ space group. This material involves both cationic ($\text{Cu}^{2+}\leftrightarrow\text{Cu}^+$) and anionic ($\text{TCNQ}^{2-}\leftrightarrow\text{TCNQ}^-\leftrightarrow\text{TCNQ}^0$) reversible redox reactions, leading to a remarkable discharge capacity of 255 mAh g^{-1} within 20 mA g^{-1} and facilitating the electrochemical transfer of multiple electrons through the synergy between redox-active organic anions and metal cations. Notably, the transformation of Cu^{2+} to Cu^+ occurs at a high voltage of approximately 3.80 V vs. Na^+/Na , and the complete reduction of TCNQ^0 to TCNQ^- takes place in the range of $3.00\text{--}3.30 \text{ V}$ vs. Na^+/Na . This elevated voltage is attributed to the robust inductive effect of four $\text{C}\equiv\text{N}$ groups present in TCNQ. However, challenges arise in the form of Cu^{2+} ions and TCNQ molecules dissolving in the electrolyte after charging, leading to rapid capacity degradation. To tackle this issue, Huang et al.^[161] devised a hierarchical nanocomposite by *in-situ* growth CuTCNQ on a three-dimensional (3D) conductive carbon nanofiber (CNFs) network. As displayed in Figure 4b, this flexible cathode, CuTCNQ/CNFs , exhibited a notable capacity of 252 mAh g^{-1} within 0.1 C and gained

exceptional reversible stability over 1200 cycles under the voltage ranging from 2.5 V to 4.1 V vs. Na^+/Na . Additionally, it achieved a 762 Wh kg^{-1} specific energy coupled with an elevated 3.2 V average potential vs. Na^+/Na , underscoring the benefits of tailored nanoarchitectures by *in-situ*-formed electroactive MOF composites demonstrate promise for high-performance cathodes in SIBs, presenting significant potential for applications requiring highly energy-efficient devices.

Additionally, Long et al. investigated the application of $(\text{H}_2\text{NMe}_2)_2\text{Fe}_2(\text{Cl}_2\text{dhhbq})_3$ and $(\text{H}_2\text{NMe}_2)_4\text{Fe}_3(\text{Cl}_2\text{dhhbq})_3(\text{SO}_4)_2$ ^[162] as cathodes for SIBs, LIBs, and PIBs, respectively, with deprotonated 2,5-dichloro-3,6-dihydroxybenzoquinone. These cathodes demonstrated favorable electrochemical properties by the redox reaction of $\text{Fe}^{3+}/\text{Fe}^{2+}$ and $\text{Cl}_2\text{dhhbq}^{3-}/\text{Cl}_2\text{dhhbq}^{2-}$ couples.

In summary, MOF cathodes for SIBs present a promising avenue for advancing energy storage technologies. Addressing challenges related to conductivity, structural stability and redox chemistry are crucial for practical implementation. Ongoing research efforts aimed at enhancing the properties of MOF cathodes, along with a deeper understanding of their electrochemical behaviors, will aid in the development of high-performance and commercially viable SIBs. The electrochemical

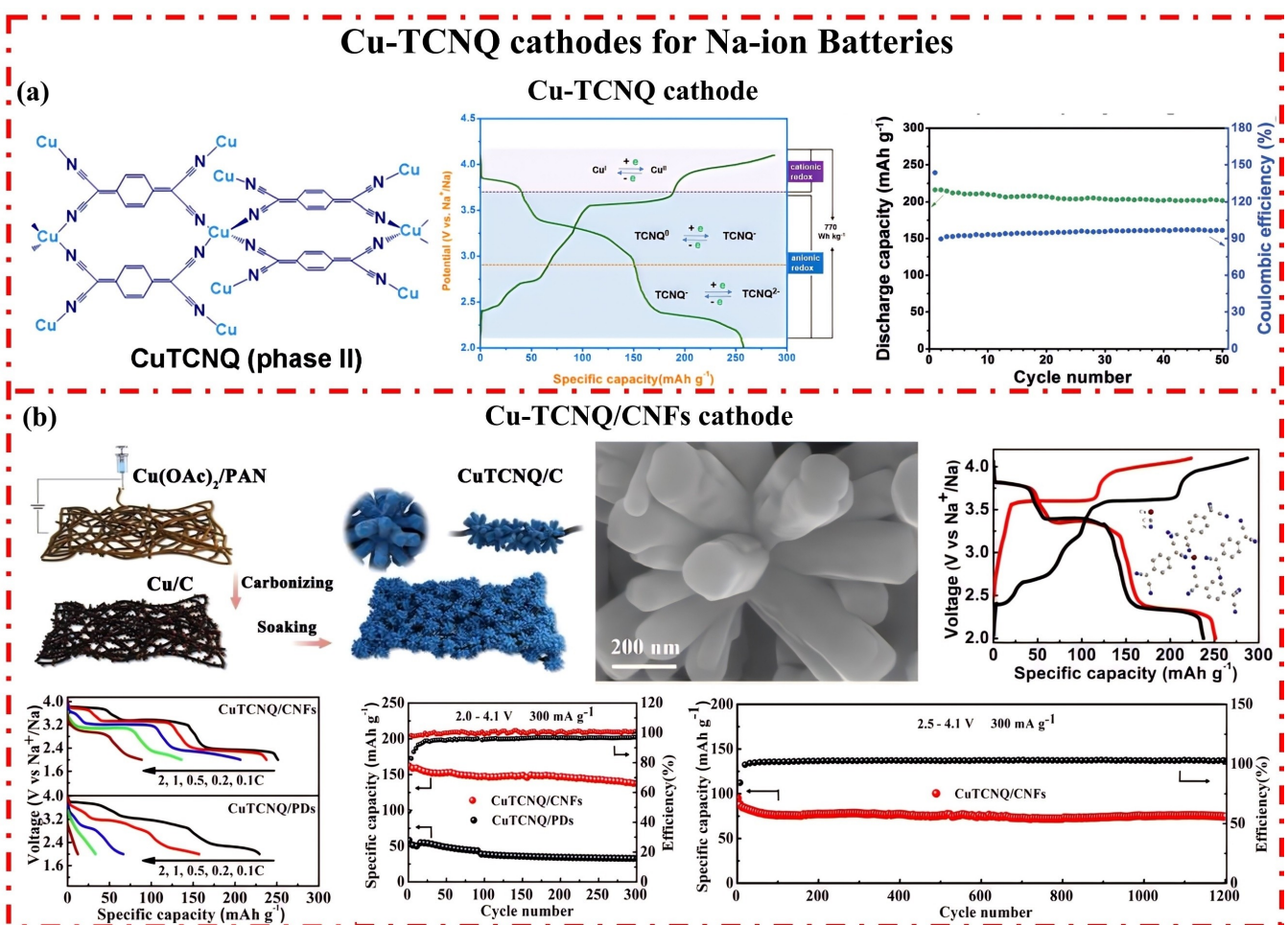


Figure 4. The structure characteristics and electrochemical performance of Cu-TCNQ cathodes for Na-ion batteries. a) Cu-TCNQ cathodes. Reproduced with permission from Ref. [160]. Copyright (2022) Elsevier. b) CuTCNQ/CNFs cathodes. Reproduced with permission from Ref. [161]. Copyright (2019) Royal Society of Chemistry.

performance overview of reported pristine MOF cathodes for SIBs is shown in Table 1.

3. Pristine MOF Anodes for SIBs

In addition to cathodes, pristine MOFs, including carboxylic acid-containing MOFs, π -d conjugated MOFs, MIL MOFs, ZIF MOFs, and others, exhibit noteworthy potential as anodes for

SIBs. Leveraging the redox reaction of transition metal ions and organic ligands, pristine MOF anodes demonstrate outstanding electrochemical performance and remarkable energy storage capabilities.

Table 1. Selected pristine MOF cathodes for Na-ion batteries.

MOF names	Crystal structure	Capacity (mAh g ⁻¹ @mA g ⁻¹)	Redox couple	Potential (V)	Ref.
PBA cathodes					
KFe ^{III} [Fe ^{II} (CN) ₆]	Fm-3m	100@0.05C	Fe ²⁺ /Fe ³⁺	2.0–4.0	[95]
Fe ^{III} Fe ^{III} (CN) ₆	Fm-3m	120@0.5C	Fe ²⁺ /Fe ³⁺	2.0–4.0	[96]
Na _{0.61} Fe[Fe(CN) ₆] _{0.94}	Fm-3m	170@25	Fe ²⁺ /Fe ³⁺	2.0–4.2	[97]
Na _{1.92} Fe[Fe(CN) ₆] _{0.08H₂O}	R-3	153@10	Fe ²⁺ /Fe ³⁺	2.0–4.2	[98]
Na _x Fe[Fe(CN) ₆]	Fm-3m	120.7@200	Fe ²⁺ /Fe ³⁺	2.0–4.2	[99]
Na _x Fe[Fe(CN) ₆]	Fm-3m	145@15	Fe ²⁺ /Fe ³⁺	2.0–4.2	[100]
K _{0.33} FeFe(CN) ₆ /RGO	Fm-3m	160@0.5C	Fe ²⁺ /Fe ³⁺	2.0–3.8	[101]
Na ₄ Fe(CN) ₆ /C	Fm-3m	87@9	Fe ²⁺ /Fe ³⁺	2.0–3.9	[102]
Na _{1.60} Co[Fe(CN) ₆] _{0.90} ·2.9H ₂ O	Fm-3m	138@75	Co ³⁺ /Co ²⁺ and Fe ³⁺ /Fe ²⁺	2.0–4.0	[104]
K _{1.84} Co[Fe(CN) ₆] _{0.89} ·□ _{0.11}	R-3 m	112@20	Co ³⁺ /Co ²⁺ and Fe ³⁺ /Fe ²⁺	2.0–4.2	[105]
Na _{1.85} Co[Fe(CN) ₆] _{0.99} ·2.5H ₂ O	R-3	128@130	Co ³⁺ /Co ²⁺ and Fe ³⁺ /Fe ²⁺	3.0–4.1	[106]
Na _{1.87} Co[Fe(CN) ₆] _{0.98} ·2.2H ₂ O	Fm-3m	151@20	Co ³⁺ /Co ²⁺ and Fe ³⁺ /Fe ²⁺	2.0–4.5	[107]
Na _{1.85} Co[Fe(CN) ₆] _{0.99} ·□ _{0.01} ·1.9H ₂ O	Fm-3m	153@10	Co ³⁺ /Co ²⁺ and Fe ³⁺ /Fe ²⁺	2.0–4.0	[108]
Na _{1.82} Ni[Fe(CN) ₆] _{0.90} ·□ _{0.10} ·2.7H ₂ O	Fm-3m	76@50	Fe ²⁺ /Fe ³⁺	2.0–4.1	[114]
Na _{1.20} Ni[Fe(CN) ₆] _{0.65}	Fm-3m	66@30	Fe ²⁺ /Fe ³⁺	2.0–4.2	[109]
K _{0.6} Ni _{1.2} Fe(CN) ₆ ·3.6H ₂ O	–	59@50	Fe ²⁺ /Fe ³⁺	3.1–3.7	[110]
K _{0.09} Ni[Fe(CN) ₆] _{0.71} ·6H ₂ O	–	70@20	Fe ²⁺ /Fe ³⁺	2.0–4.7	[111]
Na _{1.94} Ni _{1.03} Fe(CN) ₆ ·4.8H ₂ O	–	65@65	Fe ²⁺ /Fe ³⁺	3.0–3.8	[112]
KNiFe(CN) ₆	R-3 c	52@0.05C	Fe ²⁺ /Fe ³⁺	2.0–4.0	[95]
Na _{1.11} Ni _{1.03} Fe(CN) ₆ ·0.71H ₂ O	Fm-3m	90@1.1C	Fe ²⁺ /Fe ³⁺	2.0–4.0	[113]
K _{1.59} Na _{0.25} Mn[Fe(CN) ₆] _{0.89}	Fm-3m	133.3@20	Fe ³⁺ /Fe ²⁺ and Mn ³⁺ /Mn ²⁺	2.0–4.0	[115]
Na _{1.80} Mn[Fe(CN) ₆] _{0.98}	–	144@0.1C	Fe ³⁺ /Fe ²⁺ and Mn ³⁺ /Mn ²⁺	2.0–4.0	[116]
Na _{1.92} Mn[Fe(CN) ₆] _{0.98}	I2-m	152.8@10	Fe ³⁺ /Fe ²⁺ and Mn ³⁺ /Mn ²⁺	2.0–4.0	[117]
Na _{1.66} Mn[Fe(CN) ₆] _{0.94}	Fm-3m	142.7@1C	Fe ³⁺ /Fe ²⁺ and Mn ³⁺ /Mn ²⁺	2.0–4.0	[118]
Na _{1.68} Ni _{0.14} Co _{0.86} [Fe(CN) ₆] _{0.84}	P2 ₁ /n	145@30	Co ³⁺ /Co ²⁺ and Fe ³⁺ /Fe ²⁺	2.0–4.2	[119]
Na _{1.59} Mn _{0.17} Co _{0.18} Ni _{0.04} Fe _{0.61} [Fe(CN) ₆] _{0.92}	Fm-3m	113@17	Mn ³⁺ /Mn ²⁺ and Fe ³⁺ /Fe ²⁺	2.0–4.0	[120]
π-d conjugated MOF Cathodes					
Fe ₂ (DHBQ) ₃	P-1	285@50	Fe ³⁺ /Fe ²⁺ and DHBQ ²⁻ /DHBQ ⁴⁻	1.5–3.75	[145]
Fe ₂ (dobpdc)	Fd3-m	108@7	Fe ²⁺ /Fe ³⁺	2.0–3.65	[147]
Ni-TTO	–	155@100	TTO/ETT	1.2–3.0	[148]
Cu-HHTP	–	200@100	Cu ²⁺ /Cu ⁺ and HHTP ²⁻ /HHTP ⁴⁻	1.0–3.5	[149]
Zn-HHTP	–	150@100	HHTP ²⁻ /HHTP ⁴⁻	1.0–3.5	[149]
Other Cathodes					
MIL-100(Fe)	–	20@0.1C	Fe ³⁺ /Fe ²⁺	1.5–4.0	[159]
Cu-TCNQ	P2/n	255@20	Cu ²⁺ /Cu ⁺ and TCNQ ⁰ /TCNQ ²⁻	2.0–4.1	[160]
CuTCNQ/CNFs	–	252@0.1C	Cu ²⁺ /Cu ⁺ and TCNQ ⁰ /TCNQ ²⁻	2.5–4.1	[161]
(H ₂ NMe ₂) ₂ Fe ₂ (Cl ₂ dhbq) ₃	P63/mcm	170@20	Fe ³⁺ /Fe ²⁺ and Cl ₂ dhbq ³⁻ /Cl ₂ dhbq ²⁻	1.8–4.2	[162]

3.1. Carboxylic Acid-Containing MOF Anodes

As one of the typical representatives of pristine MOF anodes, carboxylic acid-containing MOFs, as exemplified within the pristine MOF anode category, are constructed with carboxylic acids and metal ions, displaying wide application as SIB anodes. Incorporating carboxylic acid as functional groups into the structure of MOFs can lead to materials with interesting properties, including potential as anodes for SIBs. The choice of carboxylic acid ligands and metal ions can affect the detailed structural and electrochemical properties of these MOFs. Recently, researchers have been typically interested in understanding and optimizing the following several key factors, i.e., electrochemical performance, structural stability, sodium-ion conductivity, and synthesis scalability when considering carboxylic acid MOFs as anodes for SIBs.

3.1.1. Characteristics and Energy Storage Mechanisms

Carboxylic acid-containing MOFs could be synthesized via various methods like solvothermal or hydrothermal processes to control the shape, size, and crystallinity of the resulted MOFs. Moreover, the choice of carboxylic acid ligands significantly impacts the structure, porosity, and electrochemical properties of the MOF.^[163,164] Concurrently, selecting appropriate metal cations for stable coordination bonds with carboxylic acid ligands is crucial. When delivered as anodes for SIBs, carboxylic acid-containing MOFs always involve the redox reactions of carboxylic acid functional groups and metal cations.^[165,166]

3.1.2. Carboxylic Acid-Containing MOF Anodes for SIBs

As for SIBs, carboxylic acid-containing MOF anodes commonly feature terephthalic acids (BDC), naphthalenedicarboxylate (NDC), biphenyl dicarboxylic acids (PBDC), and other dicarboxylic acids, along with organic ligands and metal cations like Fe, Co, Ni, Zn, etc.^[166,167] For example, as displayed in Figure 5a, the CaBDC,^[168] formed between Ca^{2+} and BDC^{2-} , was delivered as anodes for SIBs, which achieved a capacity of 235.2 mAh g^{-1} within 200 mA g^{-1} through the redox reaction of $\text{BDC}^{2-}/\text{BDC}^{4-}$ couples along with a low initial coulombic efficiency of 57.6%. Meanwhile, the ZnNDC,^[169] based on 1,4-naphthalenedicarboxylate ligands, exhibited a capacity of 200 mAh g^{-1} after undergoing 20 cycles within 40 mA g^{-1} . Moreover, as depicted in Figure 5b, Co-PBDC-400^[170] consisted of Co^{2+} and PBDC²⁻ and obtained a high capacity of 309 mAh g^{-1} within 100 mA g^{-1} after undergoing 100 cycles via pristine Co-PBDC calcining at 400°C in N_2 with 6 mol Na^+ deintercalation owing to activated sp^2 carbon in benzene rings, gaining a 68.0% initial coulombic efficiency. Furthermore, various carboxylic acid-containing MOFs based on other dicarboxylic acids, e.g., Co-TDC^[171] based on 2,5-thiophenedicarboxylic, Co-IMDC^[172] based on 4,5-imidazoledicarboxylate, Ca_2BTEC ^[173] based on 1,2,4,5-benzenetetracarboxylic acid, and Co(L) MOF/Cd(L) MOF^[174] based on 5-aminoisophthalic acid, were employed as anodes for SIBs. As the structure characteristics and detailed electrochemical performance demonstrated in Figure 5c, Ca_2BTEC gained a low coulombic efficiency of 45.8% in the initial cycle followed by stable capacities of 120 mAh g^{-1} within 20 mA g^{-1} contributed to the $\text{BTEC}^{2-}/\text{BTEC}^{4-}$ redox-active couple.

To improve the conductivity of pristine MOF anodes, high conductivity carbon nanotubes (CNTs) with high aspect ratio or high conductivity reduced graphene oxide (rGO) with high specific area was employed as conductivity additives in pristine

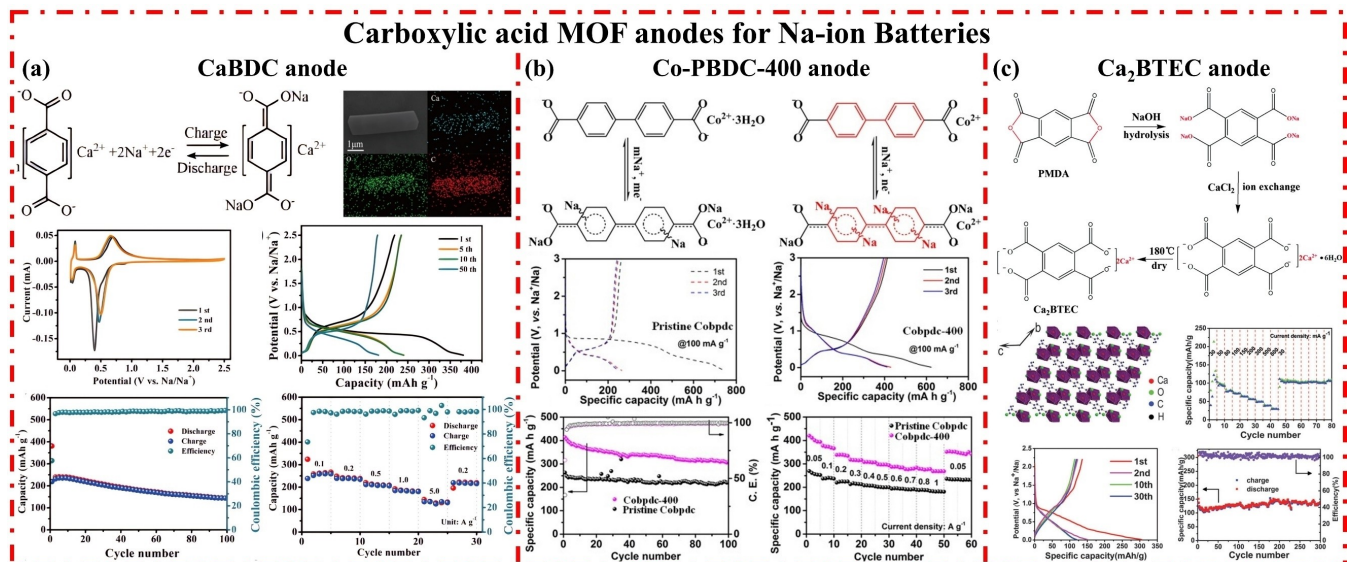


Figure 5. The structure characteristics and electrochemical performance of carboxylic acid-containing MOF anodes for Na-ion batteries. a) CaBDC anodes. Reproduced with permission from Ref. [168]. Copyright (2021) Elsevier; b) Co-PBDC-400 anodes. Reproduced with permission from Ref. [170]. Copyright (2022) Elsevier; c) Ca_2BTEC anodes. Reproduced with permission from Ref. [173]. Copyright (2016) Royal Society of Chemistry.

MOFs, resulting in high initial coulombic efficiency, high rate, and high long-cycle performance. For instance, as the research reported by Xu et al., after combining Co(L) MOF/Cd(L) MOF^[174] with rGO, Co(L) MOF/rGO and Cd(L) MOF/rGO gained higher capacities of 206 mAh g⁻¹ and 166 mAh g⁻¹ than pristine Co(L) MOF (120 mAh g⁻¹) and Cd(L) MOF (90 mAh g⁻¹) within the same current density of 500 mA g⁻¹, respectively (Figure 6a), coupled with a higher initial coulombic efficiency, exploring that carboxylate (COO⁻) and amine groups (NR₂) play a crucial role in facilitating the insertion/extraction of Na⁺ ions within the framework of Co(L) MOF/Cd(L) MOF. Meanwhile, as demonstrated in Figure 6b, the F-Co-PTA/rGO^[175] prepared by Zhang et al. with the *in-situ* synthesis of Co(No₃)₂, BDC, and rGO, showing hollow urchin nanostructures. After *in-situ* self-assembled with rGO, F-Co-PTA/rGO showed lower charge transfer resistance (RCT) and higher diffusion state of Na⁺ ions (D_{Na⁺}), resulting in a relatively higher initial coulombic efficiency of 78.0% and a better electrochemical performance with the capacities of 355 mAh g⁻¹ within 100 mA g⁻¹ and 130 mAh g⁻¹ within 2,000 mA g⁻¹, respectively.

In summary, carboxylic acid-containing MOFs as anodes for SIBs would involve in optimizing the properties of the MOFs to accommodate Na⁺ ions during charging and discharging, including considerations for the electronic conductivity, structural stability, and sodium ion diffusion within the MOF structure, however, the initial coulombic efficiencies were relatively low. Thus, the design of novel MOF structures, incorporation of conductive additives, and exploration of hybrid materials would be good choices in elevating the electrochemical performance of carboxylic acid MOF anodes for SIBs.

3.2. π-d Conjugated MOF Anodes

As motioned before, π-d conjugated MOFs are consisted of organic ligands and transition metal ions featuring oxygen,

sulfur, and nitrogen ligation sites, allowing for π electrons in a conjugated fashion and resulting in natural high-conductive. Thus, based on the redox-active C=O/C-O, C=S/C-S, or C=N/C-N couples, or along with the redox-active metal-ions, in addition to serving as cathodes, π -d conjugated MOFs have also been demonstrated the efficacy as anodes for SIBs, showcasing exceptional rate and long-cycle performance attributable to their inherent characteristics.

3.2.1. Characteristics and Energy Storage Mechanisms

As mentioned before, π -d conjugated MOFs were synthesized via solvothermal methods incorporating transition metal ions and organic oxygen, sulfur, and nitrogen ligation sites.^[176] These π -d MOF anodes, such as π -d Ni-MOF, π -d Co-MOF, and π -d Cu-MOF, leverage the redox reactions of transition metal ions or organic ligands to achieve high specific capacities and impressive rate performance in SIBs.

3.2.2. π -d Conjugated MOF Anodes for SIBs

Recently, π -d conjugated MOFs were widely employed as anodes for SIBs. Notably, as demonstrated in Figure 7a, a π -d Ni-MOF, Ni-BTA,^[177] coordinated with Ni²⁺ and planar 1,2,4,5-benzenetetramine (BTA), demonstrated a remarkable capacity of approximately 500 mAh g⁻¹ at 100 mA g⁻¹ and outstanding rate capability (330 mAh g⁻¹ within 100,000 mA g⁻¹), attributed to a three-electron (3 e⁻) reaction mechanism and structural transformations involving C=N/C-N and Ni²⁺/Ni⁺ redox active couples. Additionally, Ni-TABQ, another π -d Ni-MOF,^[178] composed of Ni metal ions and TABQ organic ligands, was designed by Bao and coworkers. Utilizing conjugated benzoid COO⁻ and C=N as the redox centers for Na-ions insertion/extraction, i.e., owing to the unique two-dimensional electron conduction and

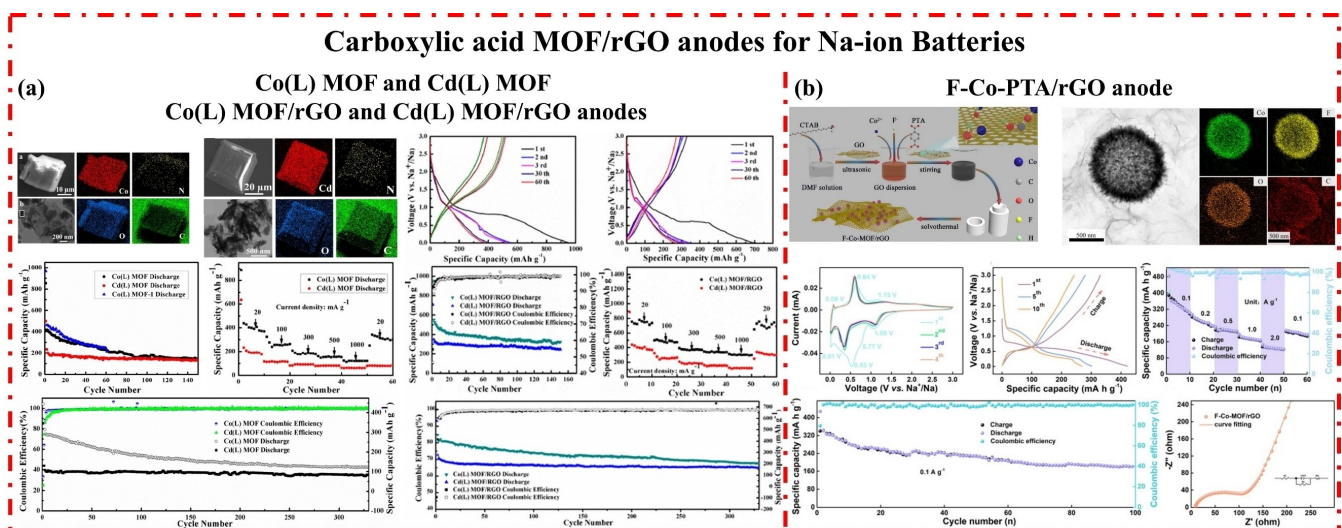


Figure 6. The structure characteristics and electrochemical performance of carboxylic acid-containing MOF/rGO anodes for Na-ion batteries. a) Co(L) MOF, Cd(L) MOF, Co(L) MOF/rGO, and Cd(L) MOF/rGO anodes. Reproduced with permission from Ref. [174]. Copyright (2017) American Chemical Society; b) F-Co-PTA/rGO anodes. Reproduced with permission from Ref. [175]. Copyright (2021) Elsevier.

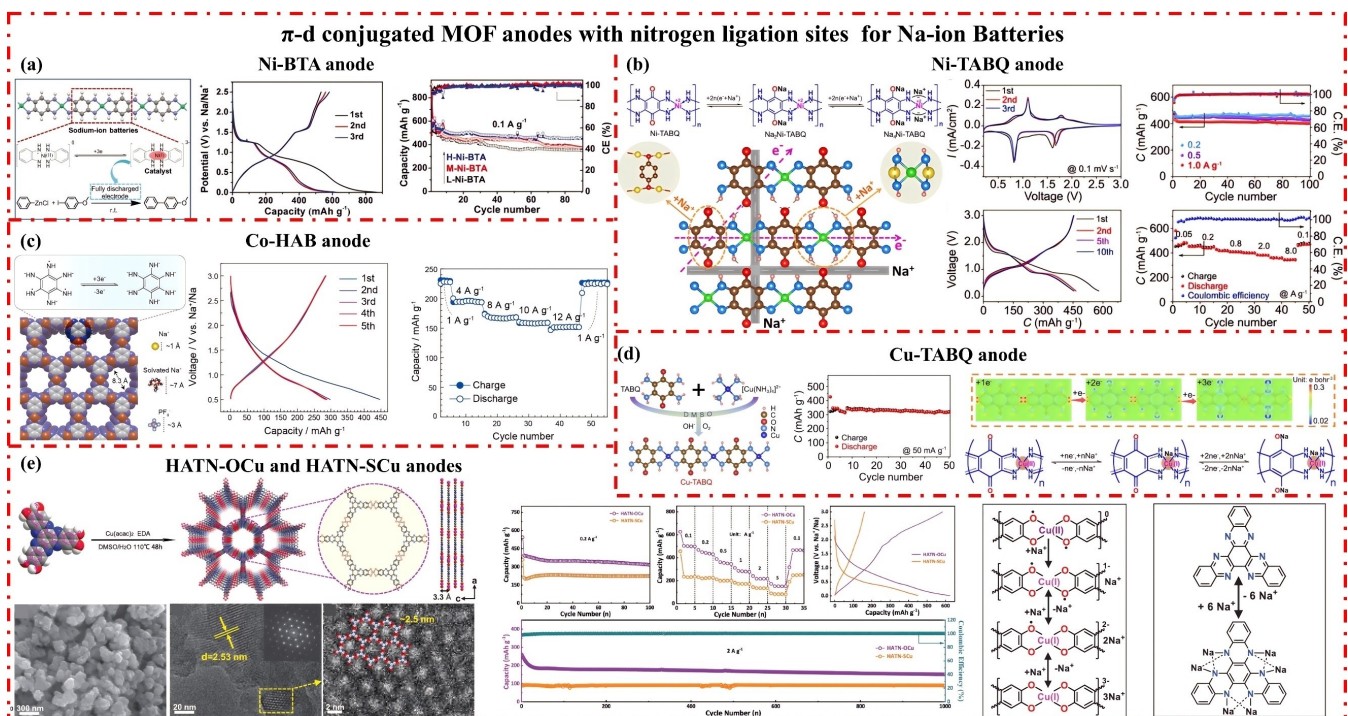


Figure 7. The structure characteristics and electrochemical performance of π -d conjugated MOF anodes for Na-ion batteries. a) Ni–BTA anodes. Reproduced with permission from Ref. [177]. Copyright (2019) Elsevier; b) Ni–TABQ anodes. Reproduced with permission from Ref. [178]. Copyright (2020) Elsevier; c) Co–HAB anodes. Reproduced with permission from Ref. [179]. Copyright (2018) American Chemical Society; d) Cu–TABQ anodes. Reproduced with permission from Ref. [180]. Copyright (2024) Royal Society of Chemistry; e) HATN–OCu and HATN–SCu anodes. Reproduced with permission from Ref. [181]. Copyright (2022) Wiley-VCH..

Na-ions diffusion pathways facilitated by the powerful Ni–N and X–H, Ni–TABQ demonstrated remarkable capacities of approximately 469.5 mAh g^{-1} within 100 mA g^{-1} and 345.4 mAh g^{-1} within $8,000 \text{ mA g}^{-1}$ sustained over 100 cycles coupled with nearly 100% coulombic efficiencies, as displayed in Figure 7b. Moreover, given the exceptional capability, π -d Co-MOF, namely Co–HAB,^[179] showcased exceptional capability to stabilize reactive hexaaminobenzene (HAB) and enable a reversible 3 e^- redox reaction per HAB. Specifically, through synthetic tunability, the bulk electrical conductivity of Co–HAB reached 1.57 S cm^{-1} , achieving an extremely high rate capability of 228 mAh g^{-1} at $1,000 \text{ mA g}^{-1}$ according to the reduction occurring on the HAB ligands instead of the Co^{2+} (Figure 7c). Furthermore, apart from π -d Ni-MOFs and π -d Co-MOFs, various π -d Cu-MOFs have been employed as SIBs' anodes. For example, as shown in Figure 7d, Cu–TABQ,^[180] synthesized via Cu^{2+} as a transition metal node and tetramino–benzoquinone (TABQ) as an organic ligand, possessing dual redox center ($\text{Cu}^{2+}/\text{Cu}^+$ and C=O/C-O), leading to a 3 e^- transfer reaction for each TABQ unit, and resulting in an extremely high reversible capacity of 322.9 mAh g^{-1} within 50 mA g^{-1} . Moreover, except for the organic ligands with oxygen and nitrogen ligation sites, sulfur could also be used as the ligation site to construct π -d Cu-MOFs. E.g., as illustrated in Figure 7e, two types π -d Cu-MOFs, namely HATN–SCu and HATN–OCu,^[181] with the different $[\text{MX}_4]$ unit ($\text{X}=\text{O}$ or S), consisted of the coordination of Cu^{2+} ions with HATN–6SR (SR: 2-ethylhexyl 2-mercaptoproacetate) and HATN–6OH (hexaazatrinnaphthylene hexahydroxyl), respectively,

synthesized by Li and coworkers. When delivered as anodes for SIBs, HATN–SCu obtained lower capacities of 224 mAh g^{-1} than HATN–OCu (317 mAh g^{-1}) according to the same current density of 100 mA g^{-1} after 100 cycles and lower initial coulomb efficiency (36.5% for HATN–SCu but 93.0% for HATN–OCu, respectively) attributed to the redox active C=N/C-N and $\text{Cu}^{2+}/\text{Cu}^+$ couples except for the redox reaction of C=O/C-O in HATN–OCu.

In summary, π -d conjugated MOF anodes for SIBs have presented a promising avenue for advanced SIBs, including relatively higher initial coulombic efficiencies, high specific capacities, and excellent rate performances and long-cycle stable abilities, attributing to that their high surface area and porous structure facilitate to improve Na-ions diffusion and storage, their naturally electrical conductivity, and their tunable nature of MOFs allows for the optimization of their chemical and structural properties, enabling the design of anodes with tailored characteristics for specific battery applications. However, there are still challenges in crystallographic structure analysis of π -d conjugated MOFs. Thus, refining these materials through enhanced conductivity, tailored pore structures, customized chemical composition, advanced characterization to further revealing detailed crystal structure and electrochemical energy storage mechanism could effectively improve the application of π -d conjugated MOFs for electrochemical energy storage devices.

3.3. Other Anodes

As for the SIBs, the pristine MIL and ZIF MOFs were rare to be used directly as anodes, but their derived materials such as alloys, metal oxide materials, metal sulfides, selenides, and phosphides were widely employed as anodes for SIBs, which have obtained higher specific capacity through alloying reaction but experiencing rapid capacity degradation due to substantial volume expansion.^[182–184]

Above all, pristine MOF anodes have gained superior electrochemical performance for SIBs, notably, the newly emerging π -d conjugated MOF anodes stand out for their high initial coulombic efficiencies, high specific capacities, impressive rate performances, and superior long-cycle stabilities owing to their inherent π -conjugated structures. Meanwhile, enhancing the conductivity of electrode composites through the use of highly conductive natural anodes and additives proves to be an effective strategy. This approach not only improves initial coulombic efficiencies but also minimizes the consumption of Na^+ ions necessary for establishing a stable solid electrolyte interphase (SEI) film. The electrochemical performance of reported pristine MOF anodes for SIBs is summarized in Table 2.

4. Summary and Outlook

Pristine MOFs, used as cathodes or anodes, including PBAs, π -conjugated MOF, carboxylic acid-containing MOF, and so on, have been demonstrated to show significant potential as electrodes for SIBs because of their high surface area, adjustable porosity, and diverse metal centers, establishing them as promising candidates for energy storage applications. However,

upon closer examination of recent studies focusing on pristine MOF electrodes, several challenges need to be addressed: 1) Low Electrical Conductivity. Pristine MOFs often exhibit low electrical conductivity, limiting their charge and discharge rates. Improving the conductivity of MOF electrodes is imperative for bolstering the overall electrochemical performance of SIBs, such as enhancing the natural conductivity of MOFs like high-conductive π -d conjugated MOFs and MOF-carbon composites with high conductivity carbon additives; 2) Structural Stability. Some MOFs may undergo structural changes during repeated cycling, leading to degradation of the electrode materials. Maintaining the structural integrity of MOFs is essential for long-term stability and cycle life of SIBs; 3) Limited Sodium Diffusion. The diffusion kinetics of sodium-ions within MOF structures can be slow, resulting in poor rate capabilities. Enhancing the diffusion properties of MOF electrodes is essential for achieving high power density in sodium-ion batteries.

Despite these challenges, there is significant potential for pristine MOF electrodes in SIBs. The following various strategies should be proposed to overcome these hurdles and unlock the full capabilities of MOFs for SIBs: 1) Conductive Additives. Incorporating conductive additives, such as high aspect ratio carbon nanotubes or high specific surface area graphene, can enhance the overall conductivity of MOF electrodes, thus improving their rate performance; 2) Structural Engineering. Designing MOFs with specific structures and functional groups can improve their stability during cycling. Rational design approaches aim to tailor MOF structures to accommodate the volume changes associated with sodium insertion/extraction; 3) Nanostructuring. Creating nano-sized MOF particles or thin films can facilitate faster sodium-ions diffusion and shorten the

Table 2. Selected pristine MOF anodes for Na-ion batteries.

MOF names	Capacity (mAh g ⁻¹ @mAg ⁻¹)	Initial Coulomb efficiency	Redox couple	Ref.
Carboxylic acid MOF Anodes				
CaBDC	235.2@200	57.6%	C=O/C–O	[168]
ZnNDC	200@40	33.0%	C=O/C–O	[169]
Co–PBDC-400	309@100	68.0%	C=O/C–O	[170]
Co–TDC	339@100	68.8%	C=O/C–O	[171]
Co–IMDC	239@20	26.1%	C=O/C–O	[172]
Ca ₂ BTEC	120@20	45.8%	C=O/C–O	[173]
Co(L) MOF	120@500	47.0%	C=O/C–O	[174]
Cd(L) MOF	90@500	40.1%	C=O/C–O	
Co(L) MOF/rGO	206@500	54.7%	C=O/C–O	
Cd(L) MOF/rGO	166@500	46.7%	C=O/C–O	
F–Co–PTA/rGO	355@130	78.0%	C=O/C–O	[175]
π-d conjugated MOF Anodes				
Ni–BTA	500@100	61.7%	Ni ²⁺ /Ni ⁺ and C=N/C–N	[177]
Ni–TABQ	469.5@100	78.4%	C=O/C–O	[178]
Co–HAB	228@1,000	64.6%	HAB ²⁻ /HAB ⁴⁻	[179]
Cu–TABQ	322.9@50	75.6%	Cu ²⁺ /Cu ⁺ and C=O/C–O	[180]
HATN–Ocu	317@100	93.0%	Cu ²⁺ /Cu ⁺ and C=O/C–O	[181]
HATN–SCu	224@100	36.5%		

diffusion pathways, addressing the slow kinetics issue; 4) Hybrid Materials. Combining MOFs with other materials, e.g., metal oxides or metal sulfides, in hybrid electrode architectures can synergistically enhance the overall electrochemical performance by leveraging the unique properties of each component.

Pristine MOF electrodes for SIBs present both challenges and opportunities. Addressing issues related to low electrical conductivity, structural stability, and sodium diffusion kinetics are crucial for realizing the full potential of MOFs in energy storage devices. Ongoing research and development efforts should be focused on material design, engineering strategies, and innovative combinations with other materials to overcome these challenges and provide the clear path for the practical implementation of MOFs in high-performance SIBs.

Acknowledgements

This work was supported by the Foundation of Sichuan University of Science & Engineering (2023RC02, 2023RC03). QZ. thanks the funding support from City University of Hong Kong (9380117 and 7020089), Hong Kong Institute for Advanced Study, City University of Hong Kong, Hong Kong, P. R. China.

Conflict of Interests

The authors declare no conflict of interest.

Keywords: Na-ion batteries • metal-organic frameworks • cathodes • anodes

- [1] J. Gao, M. He, Z. Y. Lee, W. Cao, W.-W. Xiong, Y. Li, R. Ganguly, T. Wu, Q. Zhang, *Dalton Trans.* **2013**, *42*, 11367–11370.
- [2] P. Li, F.-F. Cheng, W.-W. Xiong, Q. Zhang, *Inorg. Chem. Front.* **2018**, *5*, 2693–2708.
- [3] J. Gao, K. Ye, M. He, W.-W. Xiong, W. Cao, Z. Y. Lee, Y. Wang, T. Wu, F. Huo, X. Liu, *J. Solid State Chem.* **2013**, *206*, 27–31.
- [4] C. Li, K. Wang, J. Li, Q. Zhang, *Nanoscale* **2020**, *12*, 7870–7874.
- [5] J. Zhao, X. Liu, Y. Wu, D.-S. Li, Q. Zhang, *Coord. Chem. Rev.* **2019**, *391*, 30–43.
- [6] Y.-P. Wu, X.-Q. Wu, J.-F. Wang, J. Zhao, W.-W. Dong, D.-S. Li, Q. Zhang, *Cryst. Growth Des.* **2016**, *16*, 2309–2316.
- [7] Z.-S. Qin, W.-W. Dong, J. Zhao, Y.-P. Wu, Q. Zhang, D.-S. Li, *Inorg. Chem. Front.* **2018**, *5*, 120–126.
- [8] G. W. Xu, Y. P. Wu, W. W. Dong, J. Zhao, X. Q. Wu, D. S. Li, Q. Zhang, *Small* **2017**, *13*, 1602996.
- [9] O. Yaghi, H. Li, *J. Am. Chem. Soc.* **1995**, *117*, 10401–10402.
- [10] H. Li, M. Eddaoudi, M. O’Keeffe, O. M. Yaghi, *Nature* **1999**, *402*, 276–279.
- [11] M. Eddaoudi, J. Kim, N. Rosi, D. Vodak, J. Wachter, M. O’Keeffe, O. M. Yaghi, *Science* **2002**, *295*, 469–472.
- [12] A. Dhakshinamoorthy, A. M. Asiri, H. Garcia, *Angew. Chem. Int. Ed.* **2016**, *55*, 5414–5445.
- [13] X. Cao, C. Tan, M. Sindoro, H. Zhang, *Chem. Soc. Rev.* **2017**, *46*, 2660–2677.
- [14] B. Ghalei, K. Sakurai, Y. Kinoshita, K. Wakimoto, A. P. Isfahani, Q. Song, K. Doitomi, S. Furukawa, H. Hirao, H. Kusuda, *Nat. Energy* **2017**, *2*, 17086.
- [15] Z. Kang, L. Fan, D. Sun, *J. Mater. Chem. A* **2017**, *5*, 10073–10091.
- [16] X. Lian, Y. Fang, E. Joseph, Q. Wang, J. Li, S. Banerjee, C. Lollar, X. Wang, H.-C. Zhou, *Chem. Soc. Rev.* **2017**, *46*, 3386–3401.
- [17] J. Liu, D. Zhu, C. Guo, A. Vasileff, S. Z. Qiao, *Adv. Energy Mater.* **2017**, *7*, 1700518.
- [18] M. X. Wu, Y. W. Yang, *Adv. Mater.* **2017**, *29*, 1606134.
- [19] E. A. Dolgopolova, A. M. Rice, C. R. Martin, N. B. Shustova, *Chem. Soc. Rev.* **2018**, *47*, 4710–4728.
- [20] Q. Ren, H. Wang, X. F. Lu, Y. X. Tong, G. R. Li, *Adv. Sci.* **2018**, *5*, 1700515.
- [21] L. Yang, X. Zeng, W. Wang, D. Cao, *Adv. Funct. Mater.* **2018**, *28*, 1704537.
- [22] B. Gui, Y. Meng, Y. Xie, J. Tian, G. Yu, W. Zeng, G. Zhang, S. Gong, C. Yang, D. Zhang, C. Wang, *Adv. Mater.* **2018**, *e1802329*.
- [23] D. Vallejo-Sánchez, P. Amo-Ochoa, G. Beobide, O. Castillo, M. Fröba, F. Hoffmann, A. Luque, P. Ocón, S. Pérez-Yáñez, *Adv. Funct. Mater.* **2017**, *27*, 1605448.
- [24] L. Wang, H. Xu, J. Gao, J. Yao, Q. Zhang, *Coord. Chem. Rev.* **2019**, *398*, 213016.
- [25] Z. Wu, J. Xie, Z. J. Xu, S. Zhang, Q. Zhang, *J. Mater. Chem. A* **2019**, *7*, 4259–4290.
- [26] K. Wang, H. Wang, R. Bi, Y. Chu, Z. Wang, H. Wu, H. Pang, *Inorg. Chem. Front.* **2019**, *6*, 2873–2884.
- [27] K. Wang, X. Cao, S. Wang, W. Zhao, J. Xu, Z. Wang, H. Wu, *ACS Appl. Mater. Interfaces* **2018**, *10*, 9104–9115.
- [28] K.-B. Wang, Q. Xun, Q. Zhang, *EnergyChem* **2020**, *2*, 100025.
- [29] K. Wang, M. Zheng, X. Shi, Z. Lin, H. Wang, Y. Lu, *Chem. Eng. J.* **2015**, *266*, 141–147.
- [30] K. Wang, X. Shi, Z. Zhang, X. Ma, Y. Lu, H. Wang, *J. Alloys Compd.* **2015**, *632*, 361–367.
- [31] C. Li, J. Xue, J. Ma, J. Li, *J. Electrochem. Soc.* **2019**, *166*, A5221–A5225.
- [32] C. Li, H. Tan, J. Pei, C. Wang, C. Fan, F. Huang, B. Cao, M. Hao, Y. Li, Z. Wang, J. Li, *New J. Chem.* **2017**, *41*, 14539–14544.
- [33] Y. Qian, F. Zhang, H. Pang, *Adv. Funct. Mater.* **2021**, *31*, 2104231.
- [34] K. Wang, Y. Li, L.-H. Xie, X. Li, J.-R. Li, *Chem. Soc. Rev.* **2022**, *51*, 6417–6441.
- [35] O. M. Yaghi, G. Li, H. Li, *Nature* **1995**, *378*, 703–706.
- [36] J. Ren, Y. Huang, H. Zhu, B. Zhang, H. Zhu, S. Shen, G. Tan, F. Wu, H. He, S. Lan, *Carbon Energy* **2020**, *2*, 176–202.
- [37] a) J. Fonseca, T. Gong, L. Jiao, H.-L. Jiang, *J. Mater. Chem. A* **2021**, *9*, 10562–10611; b) H.-S. Lu, L. Bai, W.-W. Xiong, P. Li, J. Ding, G. Zhang, T. Wu, Y. Zhao, J. Lee, Y. Yang, B. Geng, Q. Zhang, *Inorg. Chem.* **2014**, *53*, 8529–8537; c) K. Wang, S. Wang, J. Liu, Y. Guo, F. Mao, H. Wu, Q. Zhang, *ACS Appl. Mater. Interfaces* **2021**, *13*, 15315–15323; d) U. Khan, A. Nairan, J. Gao, Q. Zhang, *Small Structures* **2022**, *4*, 2200109; e) Y. Pan, R. Abazari, Y. Wu, J. Gao, Q. Zhang, *Electrochim. Commun.* **2021**, *126*, 107024.
- [38] L.-F. Ma, D.-S. Li, G.-P. Yang, Q. Zhang, *Front. Chem.* **2023**, *11*, 1245159.
- [39] Y. Shen, T. Pan, L. Wang, Z. Ren, W. Zhang, F. Huo, *Adv. Mater.* **2021**, *33*, 2007442.
- [40] T. A. Goetjen, J. Liu, Y. Wu, J. Sui, X. Zhang, J. T. Hupp, O. K. Farha, *Chem. Commun.* **2020**, *56*, 10409–10418.
- [41] D. Chen, W. Yang, L. Jiao, L. Li, S. H. Yu, H. L. Jiang, *Adv. Mater.* **2020**, *32*, 2000041.
- [42] H. Konnerth, B. M. Matsagar, S. S. Chen, M. H. Precht, F.-K. Shieh, K. C.-W. Wu, *Coord. Chem. Rev.* **2020**, *416*, 213319.
- [43] M. Ali, E. Pervaiz, T. Noor, O. Rabi, R. Zahra, M. Yang, *Int. J. Energy Res.* **2021**, *45*, 1190–1226.
- [44] W. Fan, X. Zhang, Z. Kang, X. Liu, D. Sun, *Coord. Chem. Rev.* **2021**, *443*, 213968.
- [45] H. Li, L. Li, R.-B. Lin, W. Zhou, Z. Zhang, S. Xiang, B. Chen, *EnergyChem* **2019**, *1*, 100006.
- [46] H. Daglar, H. C. Gulbalkan, G. Avci, G. O. Aksu, O. F. Altundal, C. Altintas, I. Erucar, S. Keskin, *Angew. Chem. Int. Ed.* **2021**, *60*, 7828–7837.
- [47] D.-X. Xue, Q. Wang, J. Bai, *Coord. Chem. Rev.* **2019**, *378*, 2–16.
- [48] Y. Liu, X.-Y. Xie, C. Cheng, Z.-S. Shao, H.-S. Wang, *J. Mater. Chem. C* **2019**, *7*, 10743–10763.
- [49] M. S. Yao, J. W. Xiu, Q. Q. Huang, W. H. Li, W. W. Wu, A. Q. Wu, L. A. Cao, W. H. Deng, G. E. Wang, G. Xu, *Angew. Chem.* **2019**, *131*, 15057–15061.
- [50] M. Daniel, G. Mathew, M. Anpo, B. Neppolian, *Coord. Chem. Rev.* **2022**, *468*, 214627.
- [51] G. L. Yang, X. L. Jiang, H. Xu, B. Zhao, *Small* **2021**, *17*, 2005327.
- [52] L. Wang, G.-Z. Guo, M. Wang, H.-Y. Ruan, Y.-P. Wu, X.-Q. Wu, Q. Zhang, D.-S. Li, *Inorg. Chem.* **2023**, *62*, 16426–16434.
- [53] H. E. Emam, R. M. Abdelhameed, H. B. Ahmed, *J. Environ. Chem. Eng.* **2020**, *8*, 104386.
- [54] Q. Gu, H. Y. Ng, D. Zhao, J. Wang, *APL Mater.* **2020**, *8*, 040902.
- [55] M. Woellner, S. Hausdorf, N. Klein, P. Mueller, M. W. Smith, S. Kaskel, *Adv. Mater.* **2018**, *30*, 1704679.

- [56] P. M. Bhatt, V. Guillerm, S. J. Datta, A. Shkurenko, M. Eddaoudi, *Chem* **2020**, *6*, 1613–1633.
- [57] C. Gu, Z. Yu, J. Liu, D. S. Sholl, *ACS Appl. Mater. Interfaces* **2021**, *13*, 11039–11049.
- [58] F. A. Guo, J. Wang, C. Chen, X. Dong, X. Li, H. Wang, P. Guo, Y. Han, J. Li, *Angew. Chem. Int. Ed.* **2023**, *62*, e202303527.
- [59] H. Wang, S. Zhao, Y. Liu, R. Yao, X. Wang, Y. Cao, D. Ma, M. Zou, A. Cao, X. Feng, *Nat. Commun.* **2019**, *10*, 4204.
- [60] X. Ren, G. Liao, Z. Li, H. Qiao, Y. Zhang, X. Yu, B. Wang, H. Tan, L. Shi, X. Qi, *Coord. Chem. Rev.* **2021**, *435*, 213781.
- [61] X. Liang, X. Zhou, C. Ge, H. Lin, S. Satapathi, Q. Zhu, H. Hu, *Org. Electron.* **2022**, *106*, 106546.
- [62] L. T. Zhang, Y. Zhou, S. T. Han, *Angew. Chem.* **2021**, *133*, 15320–15340.
- [63] M. Ding, X. Cai, H.-L. Jiang, *Chem. Sci.* **2019**, *10*, 10209–10230.
- [64] R. Freund, O. Zaremba, G. Arnauts, R. Ameloot, G. Skorupskii, M. Dincă, A. Bavykina, J. Gascon, A. Ejsmont, J. Goscianska, *Angew. Chem. Int. Ed.* **2021**, *60*, 23975–24001.
- [65] Y. Yao, C. Wang, J. Na, M. S. A. Hossain, X. Yan, H. Zhang, M. A. Amin, J. Qi, Y. Yamauchi, J. Li, *Small* **2022**, *18*, 2104387.
- [66] C. Liu, J. Wang, J. Wan, C. Yu, *Coord. Chem. Rev.* **2021**, *432*, 213743.
- [67] Z. Ye, Y. Jiang, L. Li, F. Wu, R. Chen, *Nano-Micro Lett.* **2021**, *13*, 1–37.
- [68] V. Shrivastav, S. Sundriyal, P. Goel, H. Kaur, S. K. Tuteja, K. Vikrant, K.-H. Kim, U. K. Tiwari, A. Deep, *Coord. Chem. Rev.* **2019**, *393*, 48–78.
- [69] Y. Hu, R. Han, L. Mei, J. Liu, J. Sun, K. Yang, J. Zhao, *Mater. Today Energy* **2021**, *19*, 100608.
- [70] R. C. K. Reddy, X. Lin, A. Zeb, C.-Y. Su, *Electrochem. Energy Rev.* **2022**, *1*, 36.
- [71] X. Hou, C. Li, M. Li, Y. Liu, W. Zhu, Z. Li, Y. Xu, *Chin. J. Chem.* **2023**, *41*, 2597–2603.
- [72] A. Li, C. Li, P. Xiong, J. Zhang, D. Geng, Y. Xu, *Chem. Sci.* **2022**, *13*, 7575–7580.
- [73] M. Du, P. Geng, C. Pei, X. Jiang, Y. Shan, W. Hu, L. Ni, H. Pang, *Angew. Chem. Int. Ed.* **2022**, *61*, e202209350.
- [74] S. Zheng, Y. Sun, H. Xue, P. Braunstein, W. Huang, H. Pang, *Natl. Sci. Rev.* **2022**, *9*, nwab197.
- [75] T. Zhao, H. Wu, X. Wen, J. Zhang, H. Tang, Y. Deng, S. Liao, X. Tian, *Coord. Chem. Rev.* **2022**, *468*, 214642.
- [76] a) H. Zhou, G. Zhu, S. Dong, P. Liu, Y. Lu, Z. Zhou, S. Cao, Y. Zhang, H. Pang, *Adv. Mater.* **2023**, *35*, 2211523; b) S. Xu, J. Wu, X. Wang, Q. Zhang, *Chem. Sci.* **2023**, *14*, 13601–13628; c) Y. Guo, K. Wang, Y. Hong, H. Wu, Q. Zhang, *Dalton Trans.* **2021**, *50*, 11331–11346.
- [77] K. Chayambuka, G. Mulder, D. L. Danilov, P. H. Notten, *Adv. Energy Mater.* **2020**, *10*, 2001310.
- [78] Q. Pan, Z. Tong, Y. Su, S. Qin, Y. Tang, *Adv. Funct. Mater.* **2021**, *31*, 2103912.
- [79] Y. Zhao, Y. Kang, J. Wozny, J. Lu, H. Du, C. Li, T. Li, F. Kang, N. Tavajohi, B. Li, *Nat. Rev. Mater.* **2023**, *8*, 623–634.
- [80] Y. Yang, C. Wu, X. X. He, J. Zhao, Z. Yang, L. Li, X. Wu, L. Li, S. L. Chou, *Adv. Funct. Mater.* **2024**, *34*, 2302277.
- [81] a) C. Li, Y. Yuan, M. Yue, Q. Hu, X. Ren, B. Pan, C. Zhang, K. Wang, Q. Zhang, *Small* **2024**, 2310373; b) S. Xu, C. Wang, T. Song, H. Yao, J. Yang, X. Wang, J. Zhu, C.-S. Lee, Q. Zhang, *Adv. Sci.* **2023**, *10*, 2304497; c) J. Wang, Y. Tong, W. Huang, Q. Zhang, *Batteries & Supercaps* **2023**, *6*, e202200413; d) M. Zhang, Y. Tong, J. Xie, W. Huang, Q. Zhang, *Chem. Eur. J.* **2021**, *27*, 16754–16759; e) W. Xiong, W. Huang, M. Zhang, P. Hu, H. Cui, Q. Zhang, *Chem. Mater.* **2019**, *31*, 8069–8075; f) S. Wang, C. Sun, N. Wang, Q. Zhang, *J. Mater. Chem. A* **2019**, *7*, 10138–10158; g) J. Hu, Y. Hong, M. Guo, Y. Hu, W. Tang, S. Xu, S. Jia, B. Wei, S. Liu, C. Fan, Q. Zhang, *Energy Storage Mater.* **2023**, *56*, 267–299; h) J. Sun, Y. Xu, Y. Lv, Q. Zhang, X. Zhou, *CCS Chemistry* **2023**, *5*, 1259–1276; i) J. Xie, Q. Zhang, *Mater. Today Energy* **2020**, *18*, 100547.
- [82] J. E. Zhou, R. C. K. Reddy, A. Zhong, Y. Li, Q. Huang, X. Lin, J. Qian, C. Yang, I. Manke, R. Chen, *Adv. Mater.* **2024**, 2312471.
- [83] X. Tang, C. Liu, H. Wang, L.-P. Lv, W. Sun, Y. Wang, *Coord. Chem. Rev.* **2023**, *494*, 215361.
- [84] S. Nagappan, M. Duraivel, V. Elayappan, N. Muthuchamy, B. Mohan, A. Dhakshinamoorthy, K. Prabakar, J.-M. Lee, K. H. Park, *Energy Technol.* **2023**, *11*, 2201200.
- [85] N. Zhang, J.-C. Wang, Y.-F. Guo, P.-F. Wang, Y.-R. Zhu, T.-F. Yi, *Coord. Chem. Rev.* **2023**, *479*, 215009.
- [86] Q. Huang, A. Zeb, Z. Xu, S. Sahar, J.-E. Zhou, X. Lin, Z. Wu, R. C. K. Reddy, X. Xiao, L. Hu, *Coord. Chem. Rev.* **2023**, *494*, 215335.
- [87] V. Shrivastav, P. Dubey, S. Sundriyal, U. K. Tiwari, A. Deep, *Coord. Chem. Rev.* **2024**, *499*, 215497.
- [88] W. Zhou, Y. Tang, X. Zhang, S. Zhang, H. Xue, H. Pang, *Coord. Chem. Rev.* **2023**, *477*, 214949.
- [89] H. Zhang, J. Peng, L. Li, Y. Zhao, Y. Gao, J. Wang, Y. Cao, S. Dou, S. Chou, *Adv. Funct. Mater.* **2023**, *33*, 2210725.
- [90] M. He, R. Davis, D. Chartouni, M. Johnson, M. Abplanalp, P. Troendle, R.-P. Sutterlin, *J. Power Sources* **2022**, *548*, 232036.
- [91] J. Peng, J. Huang, Y. Gao, Y. Qiao, H. Dong, Y. Liu, L. Li, J. Wang, S. Dou, S. Chou, *Small* **2023**, 2300435.
- [92] W. Wang, Y. Gang, J. Peng, Z. Hu, Z. Yan, W. Lai, Y. Zhu, D. Appadoo, M. Ye, Y. Cao, *Adv. Funct. Mater.* **2022**, *32*, 2111727.
- [93] N. Nasir, F. Badrudin, A. Idrus, F. Sazman, M. Taib, M. Yahya, *Mol. Cryst. Liq. Cryst.* **2019**, *693*, 115–122.
- [94] J. Peng, W. Zhang, Q. Liu, J. Wang, S. Chou, H. Liu, S. Dou, *Adv. Mater.* **2022**, *34*, 2108384.
- [95] Y. Lu, L. Wang, J. Cheng, J. B. Goodenough, *Chem. Commun.* **2012**, *48*, 6544–6546.
- [96] X. Wu, W. Deng, J. Qian, Y. Cao, X. Ai, H. Yang, *J. Mater. Chem. A* **2013**, *1*, 10130–10134.
- [97] Y. You, X.-L. Wu, Y.-X. Yin, Y.-G. Guo, *Energy Environ. Sci.* **2014**, *7*, 1643–1647.
- [98] L. Wang, J. Song, R. Qiao, L. A. Wray, M. A. Hossain, Y.-D. Chuang, W. Yang, Y. Lu, D. Evans, J.-J. Lee, *J. Am. Chem. Soc.* **2015**, *137*, 2548–2554.
- [99] Y. Liu, Y. Qiao, W. Zhang, Z. Li, X. Ji, L. Miao, L. Yuan, X. Hu, Y. Huang, *Nano Energy* **2015**, *12*, 386–393.
- [100] J. Peng, W. Zhang, J. Wang, L. Li, W. Lai, Q. Yang, B. Zhang, X. Li, Y. Du, H. Liu, *Adv. Energy Mater.* **2021**, *11*, 2102356.
- [101] H. Wang, L. Wang, S. Chen, G. Li, J. Quan, E. Xu, L. Song, Y. Jiang, *J. Mater. Chem. A* **2017**, *5*, 3569–3577.
- [102] J. Qian, M. Zhou, Y. Cao, X. Ai, H. Yang, *Adv. Energy Mater.* **2012**, *2*, 410–414.
- [103] W. Zhu, A. Li, Z. Wang, J. Yang, Y. Xu, *Small* **2021**, *17*, 2006424.
- [104] M. Takachi, T. Matsuda, Y. Moritomo, *Appl. Phys. Express* **2013**, *6*, 025802.
- [105] X. Jiang, F. Hu, W. Wang, J. Qiu, X. Zheng, *J. Alloys Compd.* **2019**, *774*, 315–320.
- [106] X. Wu, M. Sun, S. Guo, J. Qian, Y. Liu, Y. Cao, X. Ai, H. Yang, *ChemNanoMat* **2015**, *1*, 188–193.
- [107] C. Li, R. Zang, P. Li, Z. Man, S. Wang, X. Li, Y. Wu, S. Liu, G. Wang, *Chem. Asian J.* **2018**, *13*, 342–349.
- [108] X. Wu, C. Wu, C. Wei, L. Hu, J. Qian, Y. Cao, X. Ai, J. Wang, H. Yang, *ACS Appl. Mater. Interfaces* **2016**, *8*, 5393–5399.
- [109] X. Bie, K. Kubota, T. Hosaka, K. Chihara, S. Komaba, *J. Power Sources* **2018**, *378*, 322–330.
- [110] C. D. Wessells, S. V. Peddada, R. A. Huggins, Y. Cui, *Nano Lett.* **2011**, *11*, 5421–5425.
- [111] Y. You, X.-L. Wu, Y.-X. Yin, Y.-G. Guo, *J. Mater. Chem. A* **2013**, *1*, 14061–14065.
- [112] X. Wu, Y. Cao, X. Ai, J. Qian, H. Yang, *Electrochim. Commun.* **2013**, *31*, 145–148.
- [113] W. Ren, M. Qin, Z. Zhu, M. Yan, Q. Li, L. Zhang, D. Liu, L. Mai, *Nano Lett.* **2017**, *17*, 4713–4718.
- [114] T. Huang, G. Du, Y. Qi, J. Li, W. Zhong, Q. Yang, X. Zhang, M. Xu, *Inorg. Chem. Front.* **2020**, *7*, 3938–3944.
- [115] Y. Liu, D. He, R. Han, G. Wei, Y. Qiao, *Chem. Commun.* **2017**, *53*, 5569–5572.
- [116] Z. Shen, S. Guo, C. Liu, Y. Sun, Z. Chen, J. Tu, S. Liu, J. Cheng, J. Xie, G. Cao, *ACS Sustainable Chem. Eng.* **2018**, *6*, 16121–16129.
- [117] F. Peng, L. Yu, P. Gao, X.-Z. Liao, J. Wen, Y.-s. He, G. Tan, Y. Ren, Z.-F. Ma, *J. Mater. Chem. A* **2019**, *7*, 22248–22256.
- [118] Z. Shen, Y. Sun, J. Xie, S. Liu, D. Zhuang, G. Zhang, W. Zheng, G. Cao, X. Zhao, *Inorg. Chem. Front.* **2018**, *5*, 2914–2920.
- [119] J. Peng, J. Wang, H. Yi, W. Hu, Y. Yu, J. Yin, Y. Shen, Y. Liu, J. Luo, Y. Xu, *Adv. Energy Mater.* **2018**, *8*, 1702856.
- [120] B. Xie, P. Zuo, L. Wang, J. Wang, H. Huo, M. He, J. Shu, H. Li, S. Lou, G. Yin, *Nano Energy* **2019**, *61*, 201–210.
- [121] X. Huang, S. Zhang, L. Liu, L. Yu, G. Chen, W. Xu, D. Zhu, *Angew. Chem. Int. Ed. Engl.* **2018**, *57*, 146–150.
- [122] C. Li, K. Wang, J. Li, Q. Zhang, *ACS Materials Lett.* **2020**, *2*, 779–797.
- [123] X. Mu, W. Wang, C. Sun, J. Wang, C. Wang, M. Knez, *Adv. Mater. Interfaces* **2021**, *8*, 2002151.
- [124] Y. Guan, J. Lai, G. Xu, *ChemElectroChem* **2021**, *8*, 2764–2777.
- [125] Z. Zhai, W. Yan, L. Dong, S. Deng, D. P. Wilkinson, X. Wang, L. Zhang, J. Zhang, *J. Mater. Chem. A* **2021**, *9*, 20320–20344.
- [126] X. Wang, M. Fan, Y. Guan, Y. Liu, M. Liu, T. N. Karsili, J. Yi, X.-D. Zhou, J. Zhang, *J. Mater. Chem. A* **2021**, *9*, 22710–22728.

- [127] R. Dong, Z. Zhang, D. C. Tranca, S. Zhou, M. Wang, P. Adler, Z. Liao, F. Liu, Y. Sun, W. Shi, *Nat. Commun.* **2018**, *9*, 2637.
- [128] K. Wang, Y. Guo, Q. Zhang, *Small Structures* **2022**, *3*, 2100115.
- [129] S. Shang, C. Du, Y. Liu, M. Liu, X. Wang, W. Gao, Y. Zou, J. Dong, Y. Liu, J. Chen, *Nat. Commun.* **2022**, *13*, 7599.
- [130] Y. Chen, M. Tang, Y. Wu, X. Su, X. Li, S. Xu, S. Zhuo, J. Ma, D. Yuan, C. Wang, W. Hu, *Angew. Chem. Int. Ed. Engl.* **2019**, *58*, 14731–14739.
- [131] L. Wang, Y. Ni, X. Hou, L. Chen, F. Li, J. Chen, *Angew. Chem. Int. Ed.* **2020**, *59*, 22126–22131.
- [132] L. B. Zasada, L. Gui, A. A. Kamin, D. Dhakal, M. Monahan, G. T. Seidler, C. K. Luscombe, D. J. Xiao, *J. Am. Chem. Soc.* **2022**, *144*, 4515–4521.
- [133] T. Chen, J.-H. Dou, L. Yang, C. Sun, N. J. Libretto, G. Skorupskii, J. T. Miller, M. Dincă, *J. Am. Chem. Soc.* **2020**, *142*, 12367–12373.
- [134] D. Feng, T. Lei, M. R. Lukatskaya, J. Park, Z. Huang, M. Lee, L. Shaw, S. Chen, A. A. Yakovenko, A. Kulkarni, *Nat. Energy* **2018**, *3*, 30–36.
- [135] J. Xie, X. F. Cheng, X. Cao, J. H. He, W. Guo, D. S. Li, Z. J. Xu, Y. Huang, J. M. Lu, Q. Zhang, *Small* **2019**, *15*, 1903188.
- [136] S. Wang, F. Huang, Z. Zhang, W. Cai, Y. Jie, S. Wang, P. Yan, S. Jiao, R. Cao, *J. Energy Chem.* **2021**, *63*, 336–343.
- [137] R. R. Kapaev, S. Olthof, I. S. Zhidkov, E. Z. Kurmaev, K. J. Stevenson, K. Meerholz, P. A. Troshin, *Chem. Mater.* **2019**, *31*, 5197–5205.
- [138] H. Li, Y. Li, X. Yang, D. Liu, X. Liu, *Appl. Phys. Lett.* **2023**, *122*, 202903, DOI 10.1063/5.0145879.
- [139] Y.-I. Yang, Z. Huang, Y.-y. Liu, D. Guo, Q. Zhang, J.-m. Hong, *J. Colloid Interface Sci.* **2023**, *629*, 667–682.
- [140] D. Xiong, X. Deng, Z. Cao, S. Tao, Z. Song, X. Xiao, W. Deng, H. Hou, G. Zou, X. Ji, *Energy Environ. Mater.* **2023**, e12521.
- [141] J. Meng, X. Liu, C. Niu, Q. Pang, J. Li, F. Liu, Z. Liu, L. Mai, *Chem. Soc. Rev.* **2020**, *49*, 3142–3186.
- [142] Y. Xiao, Y. Xiang, S. Guo, J. Wang, Y. Ouyang, D. Li, Q. Zeng, W. Gong, L. Gan, Q. Zhang, *Energy Storage Mater.* **2022**, *51*, 882–889.
- [143] M. Shanmugam, N. Agamendran, K. Sekar, T. S. Natarajan, *Phys. Chem. Chem. Phys.* **2023**, *25*, 30116–30144.
- [144] T. Wang, J. Lei, Y. Wang, L. Pang, F. Pan, K. J. Chen, H. Wang, *Small* **2022**, *18*, 2203307.
- [145] T. Cai, Z. Hu, Y. Gao, G. Li, Z. Song, *Energy Storage Mater.* **2022**, *50*, 426–434.
- [146] H. Dong, H. Gao, J. Geng, X. Hou, S. Gao, S. Wang, S. Chou, *J. Phys. Chem. C* **2021**, *125*, 20814–20820.
- [147] M. L. Aubrey, J. R. Long, *J. Am. Chem. Soc.* **2015**, *137*, 13594–13602.
- [148] Y. Wu, Y. Chen, M. Tang, S. Zhu, C. Jiang, S. Zhuo, C. Wang, *Chem. Commun.* **2019**, *55*, 10856–10859.
- [149] Y. Chen, Q. Zhu, K. Fan, Y. Gu, M. Sun, Z. Li, C. Zhang, Y. Wu, Q. Wang, S. Xu, *Angew. Chem.* **2021**, *133*, 18917–18924.
- [150] M. Shen, H. Ma, *Coord. Chem. Rev.* **2022**, *470*, 214715.
- [151] R. Zhang, Z. Zhang, J. Jiang, H. Pang, *J. Storage Mater.* **2023**, *65*, 107217.
- [152] B.-E. Channab, M. El Ouardi, O. A. Layachi, S. E. Marrane, A. El Idrissi, A. A. BaQais, H. A. Ahsaine, *Environ. Sci.-Nano* **2023**.
- [153] G. Férey, F. Millange, M. Morcrette, C. Serre, M. L. Doublet, J. M. Grenèche, J. M. Tarascon, *Angew. Chem. Int. Ed.* **2007**, *46*, 3259–3263.
- [154] G. De Combarieu, M. Morcrette, F. Millange, N. Guillou, J. Cabana, C. Grey, I. Margiolaki, G. Férey, J.-M. Tarascon, *Chem. Mater.* **2009**, *21*, 1602–1611.
- [155] A. Fateeva, P. Horcajada, T. Devic, C. Serre, J. Marrot, J. M. Grenèche, M. Morcrette, J. M. Tarascon, G. Maurin, G. Férey, *Eur. J. Inorg. Chem.* **2010**, *24*, 3789–3794.
- [156] J. Shin, M. Kim, J. Cirera, S. Chen, G. J. Halder, T. A. Yersak, F. Paesani, S. M. Cohen, Y. S. Meng, *J. Mater. Chem. A* **2015**, *3*, 4738–4744.
- [157] T. Yamada, K. Shiraishi, H. Kitagawa, N. Kimizuka, *Chem. Commun.* **2017**, *53*, 8215–8218.
- [158] T. Yamada, K. Shiraishi, N. Kimizuka, *Chem. Lett.* **2019**, *48*, 1379–1382.
- [159] D. F. S. Gallis, H. D. Pratt III, T. M. Anderson, K. W. Chapman, *J. Mater. Chem. A* **2016**, *4*, 13764–13770.
- [160] C. Fang, Y. Huang, L. Yuan, Y. Liu, W. Chen, Y. Huang, K. Chen, J. Han, Q. Liu, Y. Huang, *Angew. Chem.* **2017**, *129*, 6897–6901.
- [161] Y. Huang, C. Fang, R. Zeng, Y. Liu, W. Zhang, Y. Wang, Q. Liu, Y. Huang, *ChemSusChem* **2017**, *10*, 4704–4708.
- [162] M. E. Ziebel, C. A. Gaglioli, A. B. Turkiewicz, W. Ryu, L. Gagliardi, J. R. Long, *J. Am. Chem. Soc.* **2020**, *142*, 2653–2664.
- [163] S. Yuan, L. Feng, K. Wang, J. Pang, M. Bosch, C. Lollar, Y. Sun, J. Qin, X. Yang, P. Zhang, *Adv. Mater.* **2018**, *30*, 1704303.
- [164] X. Zhao, X. Miao, *Coord. Chem. Rev.* **2024**, *502*, 215611.
- [165] A. N. Singh, M. Islam, A. Meena, M. Faizan, D. Han, C. Bathula, A. Hajibabaei, R. Anand, K. W. Nam, *Adv. Funct. Mater.* **2023**, *33*, 2304617.
- [166] S. Qiao, Q. Zhou, M. Ma, H. K. Liu, S. X. Dou, S. Chong, *ACS Nano* **2023**.
- [167] K. Boukayouht, L. Bazzi, S. El Hankari, *Coord. Chem. Rev.* **2023**, *478*, 214986.
- [168] F. Xiao, W. Gao, H. Wang, Q. Wang, S. Bao, M. Xu, *Mater. Lett.* **2021**, *286*, 129264.
- [169] H. Fei, W. Feng, T. Xu, *J. Colloid Interface Sci.* **2017**, *488*, 277–281.
- [170] Y. Zhang, K. Chen, H. Guo, Y. Huang, W. Li, C. Wang, Y. Wang, *Chem. Eng. J.* **2022**, *433*, 133508.
- [171] Y. Ning, X. Lou, M. Shen, B. Hu, *Mater. Lett.* **2017**, *197*, 245–248.
- [172] H. Fei, Y. Lin, T. Xu, *Ionics* **2017**, *23*, 1949–1954.
- [173] Y. Zhang, Y. Niu, M.-Q. Wang, J. Yang, S. Lu, J. Han, S.-J. Bao, M. Xu, *Chem. Commun.* **2016**, *52*, 9969–9971.
- [174] C. Dong, L. Xu, *ACS Appl. Mater. Interfaces* **2017**, *9*, 7160–7168.
- [175] R. Wei, Y. Dong, Y. Zhang, R. Zhang, M. A. Al-Tahan, J. Zhang, *J. Colloid Interface Sci.* **2021**, *582*, 236–245.
- [176] J. Geng, Y. Ni, Z. Zhu, Q. Wu, S. Gao, W. Hua, S. Idris, J. Chen, F. Li, *J. Am. Chem. Soc.* **2023**, *145*, 1564–1571.
- [177] Y. Chen, M. Tang, Y. Wu, X. Su, X. Li, S. Xu, S. Zhuo, J. Ma, D. Yuan, C. Wang, *Angew. Chem. Int. Ed.* **2019**, *58*, 14731–14739.
- [178] L. Wang, Y. Ni, X. Hou, L. Chen, F. Li, J. Chen, *Angew. Chem. Int. Ed.* **2020**, *59*, 22126–22131.
- [179] J. Park, M. Lee, D. Feng, Z. Huang, A. C. Hinckley, A. Yakovenko, X. Zou, Y. Cui, Z. Bao, *J. Am. Chem. Soc.* **2018**, *140*, 10315–10323.
- [180] L. Wang, N. Liu, X. Zhao, X. Wang, T. Zhang, Z. Luo, F. Li, *Chem. Sci.* **2024**.
- [181] B. Wang, J. Li, M. Ye, Y. Zhang, Y. Tang, X. Hu, J. He, C. C. Li, *Adv. Funct. Mater.* **2022**, *32*, 2112072.
- [182] C. Lamiel, I. Hussain, H. Rabiee, O. R. Ogunsakin, K. Zhang, *Coord. Chem. Rev.* **2023**, *480*, 215030.
- [183] J.-E. Zhou, J. Chen, Y. Peng, Y. Zheng, A. Zeb, X. Lin, *Coord. Chem. Rev.* **2022**, *472*, 214781.
- [184] J. Lin, R. C. K. Reddy, C. Zeng, X. Lin, A. Zeb, C.-Y. Su, *Coord. Chem. Rev.* **2021**, *446*, 214118.

Manuscript received: March 1, 2024

Revised manuscript received: March 29, 2024

Accepted manuscript online: April 28, 2024

Version of record online: June 10, 2024